RESEARCH STUDY OF LIGHT EMISSION CAUSED BY PRESSURE FLUCTUATIONS IN ROCKET ENGINES

B. Hornstein
Physics Department

RMD Report No. 5516-F
May 1965

Final Report
1 January 1964 - 31 December 1964

Contract AF 49(638)-1279

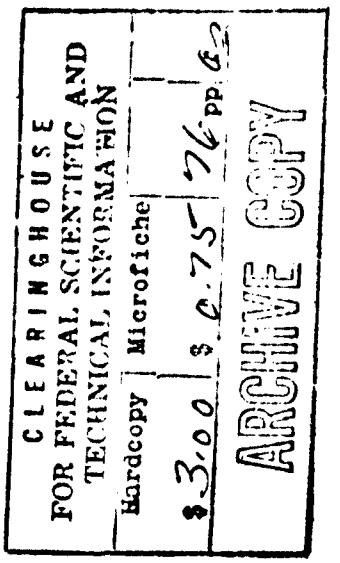

Thiokol
CHEMICAL CORPORATION
REACTION MOTORS DIVISION
DENVILLE, NEW JERSEY

RESEARCH STUDY OF LIGHT EMISSION CAUSED BY PRESSURE FLUCTUATIONS IN ROCKET ENGINES

B. Hornstein
Physics Department

RMD Report No. 5516-F
May 1965

Final Report
1 January 1964 - 31 December 1964

Contract AF 49(638)-1279

Approved by D. S. Burgess
D. S. Burgess
Manager, Physics Department

David J. Mann
D. J. Mann
Director of Research

THIOKOL CHEMICAL CORPORATION
REACTION MOTORS DIVISION
DENVILLE, NEW JERSEY

FOREWORD

This investigation was conducted under AFOSR Contract AF 49(638)-1279. Dr. B. T. Wolfson was Scientific Officer. The line of research reported here is being continued under AFOSR Contract AF 49(638)-1505 under his direction.

The author wishes to acknowledge the extensive assistance received from his associates at RMD, especially John Traylor, who contributed to nearly all aspects of the program.

ABSTRACT

Simultaneous high frequency measurements of light emission and essure were made in an oscillating premixed methane-air, 3 inch i. x 16 inch long rocket engine at pressures from 50 to 150 psig. Using tered photomultiplier tubes, emission in the OH (0, 0) band (3064A), the I (0, 0) band (4315A), and total luminosity ($CO + O = CO_2 + h\nu$) over the nge of the 1P28 phototube were monitored.

Depending on injector arrangement, longitudinal oscillations of minally 1150 cps and transverse oscillations of mainly 7100 cps and ,000 cps (1st tangential and 1st radial) were encountered. With insverse oscillations, no corresponding emission fluctuations were served, which may be owed to the aspect angle of the detectors, 90° to the gine axis (0° to the plane or pressure propagation). The longitudinal essure oscillations were always accompanied by emission fluctuations of same frequency. Emission from the chain-branching radicals OH and lagged the pressure by about . 2 milliseconds except at 150 psig where lag was zero. At 50 and 100 psig, the total luminosity was in phase h pressure.

Visible spectra were photographically recorded, and showed nilarity to previous laboratory spectra of flames as a function of essure.

These spectra and the high frequency photomultiplier data are erpreted to show that the CH and OH emission fluctuations are indicative pressure response in the early chain-branching phase of reaction. It also pears that the CH response to pressure is different for the high frequency cord and the time-averaged photographic spectrum, indicating a different etic balance under transient conditions.

During the evolution of a satisfactory experimental engine observations re made on the relationship between design and the occurrence of illations.

Although the gas-fed engine is not a true model of real-engine tability, and studies with liquid injection should be made, it is useful for optical study of kinetic aspects of the coupling processes, and as a ans for separating experimentally the component chemical and physical cesses of the complex pressure-combustion interaction.

TABLE OF CONTENTS

TABLE OF CONTENTS (Continued)

LIST OF TABLES

LIST OF ILLUSTRATIONS

LIST OF ILLUSTRATIONS (Continued)

LIST OF ILLUSTRATIONS (Continued)

1. INTRODUCTION

It was the intent of this investigation to measure spectrally resolved light emission fluctuations from an oscillating rocket engine and, by comparison of the light with the pressure fluctuations, to gain knowledge concerning important pressure-combustion interactions.

Initial concern was with kinetic interactions. To eliminate the physical processes of atomization, evaporation and mixing which are also pressure dependent, a rocket engine using a premixed gas bipropellant system was selected. This had other expected advantages. First, there was the possibility of relating results to laboratory spectroscopic investigations of flames, and systems having received the most laboratory study were in general the premixed hydrocarbon-air group. Another reason was that previous investigations (refs 1, 2) had suggested that oscillatory operation of premixed gas engines could be reasonably predictable and reproducible, which would be an experimental advantage.

Although both the Priem and Crocco models of oscillatory combustion included a pressure-sensitive component of chemical reaction as a factor in the pressure-combustion interaction, both proposed that the physical processes, being slower than chemical kinetics, were more important. Nevertheless the existence of measurable kinetic time lag was indicated by total luminosity measurements in a premix engine at Purdue (3), and gave some support to the notion that worthwhile data on the kinetic contribution could result from studies that were spectrally as well as time resolved.

If the positive slope of a pressure wave passes through a mixture undergoing reaction, evidence of increased conversion of unreacted material should be first given by increased concentrations of chain carriers or intermediates. As is known, the radicals OH, CH, and C_2 (refs 5, 6) appear as the earliest signs of reaction in hydrocarbon-air, and the time rate of change of emission from these species should be indicative of combustion rate changes. CH emission should be especially useful as its emission is entirely chemiluminescent and restricted to the reaction zone, whereas OH emission, although primarily chemiluminescent in hydrocarbon flames, is also thermally excited and therefore the excited population can be somewhat increased purely by adiabatic heating due to the pressure wave itself. Further, OH (ground state) is an equilibrium species in the products and its presence is thus not uniquely associated with the reaction zone as is CH.

The availability of narrow band interference filters at appropriate wave lengths made possible the observation of these spectral regions with photomultiplier tubes, so that adequate frequency response was available. However the question had to be resolved of whether the intensity of the CH band at 4315A was sufficiently above the underlying CO + O continuum so that the response of the photomultiplier to the filter band pass could be construed unambiguously as representing the band emission of interest. This is not self-evident merely from the filter transmission curve as the intensity of CH emission relative to background has been shown to decrease with increased pressure (ref 7) such that at 40 atm it is not discernible. The data available (ref 7) did not indicate the situation to be expected at 4 to 11 atmospheres, the pressure range of interest here.

It was assumed that we would have control through engine design over the mode and frequency of pressure oscillation. For convenience, the 1000 cps longitudinal was chosen, and based upon the Purdue experience an engine barrel of nominally 3-in. id and 16-in. length with head end injection was used, with methane-air as the propellant combination. Kistler pressure equipment and suitably filtered photomultipliers were selected for simultaneous pressure-emission fluctuation measurement. Emission was measured over the OH(0, 0) band at 3064A, the CH(0, 0) band at 4315A, and as total luminosity over the sensitivity range of the unfiltered RCA 1P28 photomultiplier.

2. EXPERIMENTAL SYSTEM

1 The Engine System

The experimental engine was a 3-inch id by 16-1/8-inch long chamber about 50-lb. thrust, run on premixed gaseous methane-air. Flow etering was by a conventional sonic orifice system which need not be scribed.

In a previous report (ref 8) a detailed description of the engine was nitted because it had not yet become apparent that combustion oscillation ould be sensitive to the construction. The necessary description is given re.

1.1 General Features

Figure 1 is an assembly drawing of the engine as originally built.

Part No. 16 is the sonic plate to decouple the premix chamber om any chamber pressure fluctuations and to prevent possible flame opagation from the chamber to the premix chamber. The sonic plate ntained six 0.1-inch diameter ports, one of which is shown in Figure 1. t indicated in this drawing are pressure taps communicating with the stream cavity of the sonic plate and the downstream annulus, which communicates with the upstream face of the water-cooled injector spool.

The sonic plate passages were later drilled out to 0.200-inch and pped so that inserts having 0.1 ports could be installed to preserve nic flow, or left out to decrease system pressure drop when the jector was rigged for sonic injection into the chamber.

1.2 Combustion Chambers

Three different combustion chambers were used:

Water-cooled, 2.85-inch id x 16-1/8-inch long
Plexiglas, 3-inch id x 1/4-inch wall x 16-1/8-inch long
Uncooled stainless, 3-inch id x 1/4-inch wall x 16-1/8-inch long.

Figure 1 shows the water-cooled and plexiglas chambers. Figures 2, and 4 are photographs of the three chambers. The bosses on the uncooled stainless chamber, Figure 4, were brazed on, and then drilled

through and tapped at those locations to accept 14 mm x 1.25 Kistler No. 628 adapters which were used to mount the Kistler pressure transducers or a sapphire window.

The water-cooled chamber, in two sections, had a 0.030-inch thick liner except where the large viewing-port bosses required solid construction. On the photograph Figure 2 can be seen one of the 1/2-inch wide by 5-1/2-inch long diametrically opposite viewing ports. Into these ports could be installed either a quartz window, or a plate with five holes tapped to receive Kistler, or Teledyne pressure sensors, and plugs in the unused holes. Both windows and metal plate can be seen in the photograph.

2.1.3 Injectors

The original injector was heavily water-cooled, and as indicated in Figure 1, passed the premixed propellants through twelve axial 0.200-inch diameter passages equally spaced on a 2.3-inch diameter circle.

The second injector used was an uncooled, solid stainless plate 0.6-inch thick with six 0.200-inch diameter axial ports evenly spaced on a 1.5-inch diameter circle.

The ports in both the water-cooled and uncooled were tapped with 1/4-20 threads to receive drilled inserts and thus vary the port diameter on the chamber side of the injector in order to control propellant injection velocity.

The photograph, Figure 5, shows the downstream face of both injectors, with an insert partially screwed home.

The gases from the cooled injector enter the chamber on a radius near the chamber wall, and from the uncooled injector, on a radius halfway between the wall and the longitudinal axis.

2.1.3.1 Gas Injection Velocities

Table I lists the calculated nominal injection velocity of a stoichiometric methane-air mixture for various injector arrangements. These velocities are for a 70°F gas stream. Actual velocities were necessarily somewhat higher owing to heat transfer from the chamber gases to the injector face and thus the gas streams, but the actual temperature rise is not known.

TABLE I

PROPELLANT INJECTION VELOCITY AT 70°F FOR VARIOUS INJECTOR - PORT ARRANGEMENTS

Injector Port Diameter, inches	Number of Ports Used			
	12 Ft/Sec	11* Ft/Sec	6 Ft/Sec	4 Ft/Sec
0.200	115	126	230	345
0.125	297	333	594	890
0.100	461	503	922	
0.070	943	1030		

*A brief series of runs with the water-cooled 12-port injector were made with one port blocked owing to seizure of a blank plug in the threads of the port.

Although the injection velocity varies with stoichiometry (i.e. the total gas flow for a given chamber pressure), it is invariant with chamber pressure at a given mixture ratio. This follows from the direct linear pressure dependence of both propellant mass flow and gas density with chamber pressure.

2.2 Instrumentation

Flow control and steady state chamber pressure instrumentation was straightforward (ref 8) and will not be discussed.

2.2.1 High Frequency Pressure Measurements

Kistler Model 601 miniature quartz pressure transducers were used, usually in a Model 628 water-cooled adapter. Crystal natural frequency

is specified at 150,000 cps, and sensitivity about 0.5 pCb*/psi. In the water-cooled adapter flat response extends to about 10,000 cps. The transducer signal was converted to a voltage by a Kistler Model 566 charge amplifier; this voltage was displayed on a Tektronix No. 551 or No. 555 oscilloscope and could be recorded on high speed tape in a central instrumentation facility. The transducers were not shock mounted.

2.2.2 High Frequency Light Measurements

2.2.2.1 Photomultiplier and Filters

In all light fluctuation measurements the radiation was viewed through a quartz or sapphire window by a RCA Type 1P28 photomultiplier tube, having the unfiltered response plotted in Figure 6. For total luminosity records, the full response was used. For monitoring the OH emission, of which the (0,0) band at 3064 is predominant, a Baird Atomic interference band pass filter was used which had the measured transmission characteristic plotted in Figure 7. Similarly, to monitor emission due to CH, a Baird Atomic interference filter having the calibration plotted in Figure 8 was used.

2.2.2.2 Optical Chamber Windows

Combustion chamber emission was viewed either through the quartz window, of 1/2-inch by 5-1/2-inch clear area, of the water-cooled chamber (Figure 2) or through a sapphire window, mounted in a modified Kistler water-cooled adapter, with the uncooled metal chamber. The Kistler-mounted window was particularly useful; by using the water-cooled adapter for both pressure and window, any combination of pressure and light measurements could be made by mounting the fittings in any of the six identical tapped holes (Figure 4).

Figure 9 is an exploded view photograph of the No. 628 adapter, unmodified, with transducer, and modified, with the 1/4-inch diameter x 2 mm thick Linde sapphire window. As can be seen, the only modifications needed were of the flame cap and the spacer tube.

---

*pico Coulomb

This sapphire window assembly has proved most satisfactory, having survived about 200 2 to 3-second runs without failure of the window and without even changing window sealing gaskets.

2.2.2.3 Photomultiplier Field of View

At the aspect angle of 90° with respect to the engine longitudinal axis, the photomultiplier responded to emission from a volume of gas within a solid angle of 10 degrees and 3-inches in length. The length corresponded to the chamber diameter.

The angular field of view was defined by field stops of blackened, drilled brass sheet; in the case of the Kistler-mounted sapphire window the stops were formed by the Kistler adapter structure itself.

At the chamber wall opposite the window, the longitudinal length corresponding to this field was 0.7 inches. With the local velocity of sound in the chamber gas on the order of 3×10^3 ft-sec^{-1}, the time required for a pressure pulse to traverse the photomultiplier field of view was about 3×10^{-5} sec. This represents the minimum pressure-light signal lag that can be resolved for a longitudinal mode, and is about 1/30 the period of a 1000 cps frequency.

2.2.2.4 Photomultiplier Sensitivity Levels

Because only relative emission intensities were sought in the light measurements, a difficult absolute calibration of the several photomultiplier-filter-field stop combinations was not made.

However, irradiance levels at the tube varied according to whether OH, CH, or total luminosity measurements were made owing to differences in spectral intensity vs wavelength, filter bandwidth, and filter transmission. Therefore the sensitivity or gain of the photomultiplier was adjusted according to which wavelength interval was being monitored so that tractable signal levels were obtained.

A Farrand Optical Company adjustable battery power supply enabled the phototube to operate linearly over a wide sensitivity range. Three standard sensitivity levels were selected and set by illuminating the desired photomultiplier-filter combination with a standard lamp through a standard field stop arrangement, and by adjusting the power supply until the desired DC tube output signal level was obtained.

2.2.3 Recording of Data

There is nothing like an oscilloscope for observing high frequency wave forms with high time resolution. The pressure and light data for all runs were displayed on a dual-beam Tektronix oscilloscope, either a Model 551 or a Model 555. For nearly all runs, a photographic record of a single sweep was made.

The obvious shortcoming of an oscilloscope record is that only a small fraction of a run can be recorded with high resolution. A small number of runs were completely recorded at 60 inches sec^{-1} on tape, the recording and playback system having flat response to 10,000 cps. The tape was not used more extensively because:

(1) The remote location of the tape system resulted in ground loop and noise problems which were a nuisance.

(2) Although confirming that pressure oscillations were of varying amplitude during a run, the complete record yielded no apparently useful information beyond that obtained from the oscilloscope record.

3. EXPERIMENTAL RESULTS

3.1 Occurrence of Instability

The occurrence and mode of combustion oscillation was more sensitive than anticipated to details of engine construction, injector geometry, and gas injection velocity. Because the main interest was in studying the relationship between pressure oscillation and light oscillation, the effect of these factors on pressure oscillation was not fully explored in that complete instability maps for all engine variables were not attempted. The main effects are described in this section.

With low injection velocity as in 12 x .200 (115 fps) injection* unstable operation was not encountered at any mixture ratio at chamber pressures between 50 psig and 150 psig in the water-cooled chamber.

At around 300 feet per second injection velocity, chamber pressure oscillations were evident in the uncooled metal chamber but not in the water-cooled chamber. Fig. 11 is a partial instability map for 11 x .125 (333 fps) injection in the uncooled metal chamber.

An instability map was not made for 6 x .2 (230 fps) injection. A small number of runs showed weak 1200 cps oscillations at 50 and 100 psig, and an O/F ratio of 10 (stoichiometric), but there were no oscillations at 50 psig and O/F of 9, nor at 100 psig and O/F of 8 and O/F of 12.

A 600 feet per second velocity, 6 x .125 (593 fps) injection resulted in pronounced longitudinal oscillations whose peak to peak amplitude was about 20% of the base chamber pressure. These were found at chamber pressures of 50 and 100 psig, and at O/F ratios from 8 to 12, the only conditions tested. Only the uncooled metal chamber was operated with this injection velocity.

---

*This notation describes an injector having 12 ports of 0.200-inch diameter giving nominally 115 feet per second port exit velocity. See Table I, Section 2.1.3.1.

With sonic or near sonic injection, chamber oscillations were found with all chamber constructions. Figure 12 is an instability map for the uncooled metal chamber with 12 x .070 (943 fps) injection. Of particular note is that pressure oscillations were encountered at all pressures and O/F ratios run, which included most of the O/F range from the rich limit (O/F = 6.2) to the lean limit (O/F = 17.5) and the pressure range 30 psig to 150 psig.* The water-cooled chamber with 12 x .070 (943 fps) showed behavior similar to that of the uncooled metal chamber at pressures greater than 100 psig but with a lower incidence of chamber oscillation at lower pressures.

With 6 x .100 (922 fps) sonic injection, reliable oscillations of 20% amplitude were obtained at chamber pressures of 50 to 150 psig and an O/F of 10, in the uncooled metal and water-cooled chambers. As this configuration was evolved towards the end of the contract period, and as our emphasis was on light emission measurements, O/F variation has not as yet been made.

Non-uniform sonic injection patterns were briefly tested with the hope of simplifying the normally complex structure of the transverse modes. The configurations used were designated 4 x .125 (890 fps) A, 4 x .125 (890 fps) B, and 4 x .125 (890 fps) C and diagrammed in Figure 10. In addition to making ignition more difficult, the instability regions were greatly altered. The B configuration showed no instability, the C configuration oscillated only at high pressure and fuel-rich, while the A configuration showed a larger, instability region although still restricted to high pressure, fuel-rich operation. All runs made are plotted in Figure 13.

The effect of configuration on wave form will be considered later.

3.2 Acoustic Isolation of the Chamber

Acoustic isolation of the chamber from the feed system is required for true high frequency oscillations. Figures 14(a), 14(b) and 14(c) corroborate that sonic injection is necessary in a gas-fed engine to attain this.

These figures show simultaneous high frequency pressure measurements taken with a flush-mounted transducer in the chamber, and a transducer exposed via a 5-1/2 inch long pressure tap to the propellant manifold cavity at the upstream face of the injector (see Fig. 1).

---

*At higher chamber pressures, air supply system pressure precluded running at the higher O/F ratios.

In Figure 14(a) the 6 x .200 (230 fps) uncooled injector permits a weak 1200 cps chamber oscillation (P_c) to drive an injector manifold oscillation (P_i) of the same frequency and amplitude, with a phase shift of about 0.6 ms (or about 270° lag). This measured time lag in the P_i signal corresponds to an estimated .625 ms transit time of an acoustic pressure pulse traveling upstream from the P_c pickup, through the injector and pressure tap, to the P_i pickup.

Figure 14(b) shows, for 11 x .125 (333 fps) injection, the 1200 cps longitudinal component of the complex P_c waveform propagating through the injector. The P_c oscillation also shows the first tangential (about 7000 cps) and a small component of the first radial (about 14,000 cps) modes, and apparently these latter oscillations are influencing the P_i waveform. In this figure the 1200 cps component in the P_c trace cannot be resolved well enough to compare with the P_i waveform. From other data that is more clear in this respect, the oscillation amplitude of the P_i 1200 cps component is consistently about 25% of the 1200 cps component in the P_c waveform, and the time lag P_c-P_i is again about .6 ms.

With 6 x .125 (594 fps) injection, once more the P_c which is predominately 1200 cps longitudinal is accompanied by a P_i 1200 cps oscillation, which has an amplitude about 25% that of P_c, and with the characteristic 0.6 ms time lag.

Sonic injection with the 6 x .100 (922 fps) injector arrangement, Figure 14(c) shows effective acoustic isolation of the chamber inasmuch as the definite 1200 cps longitudinal P_c oscillation has no counterpart in the P_i record. There is a 450 cps fluctuation in the P_i record for which we have no clear explanation. This type of P_i fluctuation was also seen in cold flow tests and thus does not appear to derive from the combustion process in the chamber.

3.3 Frequency and Mode of Oscillation

Although the frequency and mode of chamber oscillation was somewhat influenced by injection velocity (compare Figures 11 and 12), it was the diameter of the injector port circle that primarily controlled the oscillation mode.

The 12-port and 4-port arrangements, on a 2.3-inch diameter circle, injected propellant near the wall of the 3-inch i.d. chamber, and excited primarily transverse modes, except for low chamber pressures where the longitudinal was predominant. Where the transverse modes predominated, there was nearly always present a clearly audible 1000 cps- 1200 cps component, which was often but not always apparent in the oscilloscope photograph records.

The 6-port arrangement, on a 1.5-inch diameter circle, which injected propellant midway between the chamber axis and the wall, promoted in all cases the longitudinal mode. This is in accordance with the general relationship between zones of high heat release rates and the pressure pattern.

3.3.1 Identification of Modes

Identification of modes can be made from the frequency because of the large aspect ratio of the engine. Estimated frequencies for various modes are listed in Table II.

TABLE II

APPROXIMATE FREQUENCIES FOR OSCILLATION MODES IN THE 3-INCH DIAMETER X 16 INCH LONG CHAMBER

Mode	Approximate Frequency cps
1st Longitudinal	1,150
1st Tangential	7,100
1st Radial	14,000
2nd Tangential	11,000

Possible ambiguity could exist between the first radial and second tangential, but the first longitudinal and first tangential present no identification difficulty with single-pickup frequency measurements.

More positive identification can be made with dual simultaneous pressure sensing. Figures 15(a), 15(b), and 15(c) are representative oscilloscope photographs made with two Kistler transducers, mounted 180 degrees apart on a plane normal to the engine axis and 2.80 inches downstream of the injector face.

Figure 15(a) clearly identifies a longitudinal oscillation of 1150 cps. As expected, the waveforms as measured 180° apart are nearly perfectly in phase, indicating a plane wave normal to the axis. This close phasing is important to the interpretation of pressure-emission measurements, described later, which were made at the same locations.

Figure 14(b) identifies a 1200 cps longitudinal with superimposed transverse modes. A definite 7100 cps component, 180° out of phase on the two traces, is the first tangential. Modifying the 7100 cps waveform is a weak component, about double this frequency and in-phase on the two pressure traces, which is the first radial mode. The in-phase property makes this assignment unmistakable.

Figure 14(c) shows the same modes and frequencies as Figure 14(b), but with the transverse modes strong compared to the longitudinal, and with the first radial mode more pronounced. This figure also shows evidence of a phase shift between the 7100 first tangential and 14,000 first radial.

3.3.2 Waveforms

Waveforms of the longitudinal mode were generally consistent from run to run. The transverse oscillations were usually complex, and the complexity varied with respect to both the number and phasing of components.

3.3.2.1 The Longitudinal Wave

The longitudinal wave when dominant had a consistent form similar to that in Figure 15(a) and as shown in the other 1000-1200 cps oscillation records in this report. The two spikes on the rising slope correspond to the passage of a shock type wave front travelling upstream to the injector and returning downstream, after reflection from the injector face, past the flush mounted pickup.

The hash on the longitudinal waveform especially with 6-port injection may be either real pressure fluctuations in the gas, or may be mechanical vibrations in the metal parts of the system since the Kistlers were not shock mounted. It is hoped to resolve this in the future.

3.3.2.2 The Transducer Waves

Most of the transverse waveforms were of a complexity similar to that in Figures 15(b) and 15(c), that is two components, the first tangential and first radial. There were variations from run to run, and within a run, in the relative amplitudes and relative phases of the components.

Figure 16(a) shows another well defined wave pattern whose pattern is that of a first and second harmonic with a fundamental frequency of 6100* cps. Thus this too is a first tangential and first radial. Near the end of the trace, however, a third component is entering which gives the wave the appearance of containing a fourth harmonic. This could be the second radial at an estimated 28,000 cps.

Figure 16(b) is a detail of a three-component waveform with a fundamental frequency of 7100 cps. Three-component systems were frequently encountered.

Figure 16(c) shows a steep shock type high frequency form encountered in only one series of experiments using 4 x .125 (890 fps) A injection. Attempts to reproduce it for possible study as a "simple" structure failed. The measured frequency of 19,000 cps is difficult to assign to an oscillation mode without the aid of another simultaneous pressure trace.

Also found on occasion were simple sinusoidal pressure traces of about 12,000 cps.

3.4 Light Emission Fluctuation Measurements

3.4.1 Transverse Modes

With the photomultiplier aspect angle of 90 degrees with respect to the engine axis no light emission fluctuations in the OH band, the CH band or in total luminosity, were observed which were related to the transverse modes of pressure oscillation.

High time resolution as in Figure 16(b) generally showed no emission features. Figures 17(a) and 17(b) at medium time resolution show no features related to the dominant 7000 cps frequency, although in Figure 17(a) there is a suggestion of some response in the total luminosity to a 1200 cps longitudinal component.

---

* This frequency is in inconsistent with the value usually measured, about 7000 cps.

Low time resolution as in Figure 17(c) shows typical long period and andom emission fluctuations.

Thus no information was gained concerning the effect of transverse ressure oscillations on emission. This is believed due to the aspect angle. 'ith this viewing geometry, regions of high and low emission would move vay from and to the detector, but always remain in the field of view. Since .e detector integrates all emission from the volume it sees, it is probable iat the total emission over the optical path was essentially constant* even iough the spatial, or radial distribution of emission intensity may have ıried with pressure.

4.2 Longitudinal Mode

For longitudinal oscillations, light emission fluctuations were regarly observed, which were directly related to the pressure oscillations.

Figures 18 through 22 show light emission fluctuations of the same equency as the longitudinal pressure oscillations, and in definite phase lationship. This is found for the OH (3064A), the CH (4315A) and the tal luminosity band widths. Figures 18 and 19 are results for subsonic jection, 11 x .125 (333 fps) and 6 x .125 (594 fps) respectively. Figures through 22 are results for sonic injection, 6 x .1 (922 fps), of a stoiiometric mixture ratio at chamber pressures of 50 psig, 100 psig, and 0 psig.

The pressure pickup and photomultiplier were located 180 degrees art on the same plane, normal to the engine axis, 2.80 inches downream of the injector face.

Table III is a tabulation of data taken primarily from those figures owing the amplitude and phase relationship of the observed pressure d emission fluctuations.

---

s determined by the irradiance at the photomultiplier photoemissive urface.

3.4.2.1 Shape of Emission Fluctuation Trace

Reference to Figures 18 through 22 reveals two definite trends in the shape of the emission trace.

The first is the difference, for both subsonic and sonic injection, between the total luminosity trace, and the OH and CH traces. The total emission trace shows pronounced fine structure on the basic 1100-1200 cps frequency which has a qualitative resemblance to the fine structure in the corresponding chamber pressure trace, especially the noticeable shock spikes on the rise of the pressure trace.

The OH and CH emission are distinctly different from the total luminosity . Such fine structure does not appear for subsonic injection, and for sonic injection is much less pronounced than for total luminosity. Although the OH and CH fine structure seems to increase somewhat with pressure in the case of sonic injection, the trace shape as a whole retains its distinctive character compared to total luminosity. In addition and contrary to the total luminosity trace, the OH and CH traces for subsonic injection have almost exactly the form of a "smoothed" chamber pressure trace.

Particularly striking is the parallel shape between injector upstream pressure, P_i, and the CH emission seen in Figure 19(a), especially with the assumption that the chamber emission trace is lagging the P_c trace.

With sonic injection at 50 and 100 psig chamber pressure the OH and CH traces, except for the appearance of fine structure, still follow the P_c smoothed wave form more closely than does the total luminosity. At 150 psig, this is less true.

The second difference, alluded to above, is the appearance of fine structure in the OH and CH emission traces for sonic injection.

The OH trace fine structure appears related to the two major shock spikes in the pressure trace, and the relative amplitudes of the emission "spikes" are similar to those of the pressure spikes for all three chamber pressures.

The CH emission trace appears in like manner to reflect the pressure trace at 50 and 100 psig, but is different at 150 psig in that several individual cycles show the earlier CH emission peak to be substantially higher than the second, which is opposite to the main trend in the chamber pressure trace.

.4.2.2 Phase Relationship of Pressure and Light

The time lags of the emission peaks with respect to the pressure peaks, as measured from the oscilloscope records, Figures 18 through 22, are listed in Table III and are of the order 0.0 to 0.3 milliseconds.

The tabulated values may be in error by an estimated 0.1 millisecond owing to the following:

Actual error in making linear measurements on the photograph

Less than perfect synchronization of the two spots on the oscilloscope

Subjective error in selecting the peaks of the traces.

An additional source of error occurs if the pressure wave plane is not exactly normal to the axis as assumed and as usually found (see Fig. 15).

In principle these errors could be minimized by using a faster sweep, expanding the time scale. In practice the fine structure on the pressure trace, when expanded, made the selection of pressure peak sufficiently ambiguous to preclude any true advantage.

In any case, based upon the data presented in the figures and similar data not included in this report, the following statements can be made, which are either self-evident from the data presented or which appear probably correct on the basis of a larger data sample:

(a) The band emission fluctuations (OH and CH) show a regular relationship to the pressure fluctuations.

(b) At chamber pressures of 50 psig and 100 psig, the OH and CH band emission lags the chamber pressure regularly by about 0.2 ms (about one quarter period).

(c) At 150 psig, the OH and CH band emission becomes less regularly related to the pressure and are on the average in phase with the pressure, i.e., the time lag is zero.

(d) The total luminosity fluctuations, unlike the band emission, are on the average in phase with the pressure at 50 psig and 100 psig, and there is greater cycle-to-cycle variation in the pressure-emission phasing.

(e) In these data no measurable systematic difference in phase relationship, for band emission or total luminosity, accompanies a change from subsonic to sonic injection velocity.

3.4.2.3 Modulation of Pressure and Emission

In Table III are tabulated some values of the fractional modulation of chamber pressure and light emission. These are defined as:

$$\frac{\text{Peak-to-peak pressure variation}}{\text{Average chamber pressure}}$$

$$\frac{\text{Peak-to-peak photomultiplier output variation}}{\text{Average photomultiplier output.}}$$

Photomultiplier sensitivity was set at a standard level for each bandwidth of interest, although not the same level for all bandwidths. Thus, the millivolt amplitude of say the OH emission cannot be compared to the millivolt amplitude of the CH emission, but the various OH millivolt levels can be compared from run to run, and so forth.

The pressure modulation of the longitudinal oscillation was consistently about 20% for all runs near stoichiometric O/F, with a tendency to drop to around 15% at 50 psig for sonic injection, and lower for subsonic injection at this pressure.

The sets of runs from which reliable emission modulation values could be derived was limited to stoichiometric mixtures, 6 x .100 (922 fps) injection, at 50, 100, and psig A larger set of data is needed to verify the indicated trend for the set of data, summarized in Table III which is that:

Modulation of OH emission is independent of pressure

Modulation of CH and total luminosity emission increases with pressure.

PRESSURE AND LIGHT EMISSION FLUCTUATIONS FOR LONGITUDINAL OSCILLATIONS

Figure No.	Emission Band	Mean Chamber Pressure	Mean Emission Level*	Fluctuation Chamber Pressure	Amplitude Emission	Fractional Chamber Pressure	Modulation Emission	Pressure-Emissio Time Lag
		Psig	mv	Psi	mv			milliseconds
18a	OH	50	Not measured	4	10	.08	Not determined	.2
b	CH	50	"	5	60	.10	"	.3
c	Total	50	"	3	120	.06	"	0 to .2
19a	CH	100	"	20 (est)	250	.20 (est)	"	.4 (after P_i* Peak
b	CH	100	"	20	400	.20	"	.3
c	CH	100	"	30	500	.30	"	.2
20a	OH	50	125	6	30	.12	.24	.1 to .2
b	CH	50	1000	10	400	.20	.40	.2 to .3
c	Total	50	150	8	75	.16	.50	0 to .1
21a	OH	100	1500	20	400	.20	.27	.3
b	CH	100	300	20	200	.20	.67	.2
c	Total	100	150	20	100	.20	.67	0
22a	OH	150	1000	30	250	.20	.25	0
b	CH	150	200	30	200	.20	1.00	0

* Directly measured if the DC rather than AC emission level was recorded at high time resolution, or inferred from a separate run at the same conditions where the DC level of emission for the entire run was recorded and the mean level determined.

**Injector upstream pressure.

3.5 Visible Spectra

A set of spectrograms were taken of the visible radiation from the gases inside the water-cooled chamber at stoichiometric O/F ratio (O/F = 10) and at chamber pressures of 50, 100, and 150 psig. An astigmatic Hilger and Watts Raman Spectrograph with glass optics was used.

The slit of the spectrograph was parallel to the engine axis, and the system was focussed so that the image of the 5-1/2 inch clear length of the quartz window (see Figure 2, window and cover plate below engine) just filled the length of the slit.

Two spectra at each chamber pressure were photographed on a single Kodak Spectrographic Plate Type I-F. Exposure time was 2-1/2 seconds in all cases. Effective exposure at the plate was varied by using two slit widths, 100μ and 200μ , at each chamber pressure.

Prints of the six spectra are reproduced in Figure 23, violet to the left.

As the spectrograph is astigmatic, the spectra are spatially resolved along the engine axis and show the spectrum vs axial length of the chamber over the distance 1.9 inches to 7.4 inches downstream of the injector face. That is, at any wavelength, every point along a vertical line in the spectrogram corresponds to an equivalent point along the chamber length. For example, the vertical length of the sodium doublet represents the 5-1/2 inch clear length of the quartz window. In each spectrum, the bottom of the sodium line represents the upstream end of the window, 1.9 inches from the injector, and the top of the sodium line represents the downstream end of the window at 7.4 inches.

3.5.1 Spectral Features

The main features of the spectrum are:

(a) The CH(0, 0) band, at 4315A degraded to the violet

(b) The underlying CO + O continuum in the region 4000 to 4700A (approximately) whose intensity increases with pressure

(c) The sodium line(s) at 5890A, arising from trace contamination

(d) The oddly striated continuum in the vicinity of the sodium line, which has the apparent spectral distribution of a grey body.

3.5.1.1 The CH Band and the CO + O Continuum

Figure 23 shows that over the pressure range here considered (up to 150 psig) the CH band intensity is greater than that of the underlying continuum. The strong head occupies a band width of about 15A with a weaker structure discernible to about 4250A on the original negative.

The significance with respect to our instrumentation is that at 150 psig the CH emission has not become submerged in the continuum as is reported to occur at 40 atmospheres for methane-air (ref. 7). This confirms the experimental validity of relating emission fluctuations in the 4315A region to variations in CH emission rather than to variations in CO + O emission, which represent different kinetic steps in the combustion.

Other aspects of the relative band and background intensities are presented in Section 3.5.2 and discussed in Section 4.

3.5.1.2 The Striated Continuum Near The Red

A grey body continuum at the longer wavelengths immediately suggests the presence of incandescent solid carbon particles, but this is contradicted by two considerations. One is that premixed methane-air flames even at high pressures do not show carbon emission at the stoichiometric point (ref. 7). The other is that there was no visible luminosity during the runs when looking through the nozzle into the combustion chamber (by mirror).

A more likely origin for this continuum is that it is grey body emission from the combustion-heated surface of the metal cover plate containing pressure pickups and blank plugs (see Figure 2, plate and fittings above chamber) which is directly opposite the quartz window and thus in the field of the spectrograph. This is consistent with the striations, which are regular and whose position is invariant in all the spectra.

If this were true, then the striations should represent areas of varying temperature showing sharp discontinuities. Figure 24 is a drawing of the metal cover plate showing the location of fittings and plugs, with the outline of the window clear area superimposed, in juxtaposition with an enlargement of the 150 psi, 100μ spectrogram in the vicinity of the sodium line. The enlargement is such that the sodium line is now the same length as the window length.

Although with this degree of enlargement edge definition is degraded, it is still apparent that, especially towards the injector, the dark stria coincide with plugs or fittings, and the bright stria with cover plate areas between them. This confirms the cover plate assembly to be the origin of the striated continuum.

The confirmed absence of carbon particles is of value in simplifying the interpretation of densitometric measurements on the original spectra, since extinction and scattering by particles does not need to be considered.

3.5.1.3 Location of Combustion Zone

The reaction zone of the methane air system is reliably defined by the presence of CH and CO + O emission. In the spectra, Figure 23, the reaction zone as so defined does not extend the full axial length of the chamber window. Measurements on these spectrograms (linear distance and densitometric) show the following, assuming combustion ends where the CH band is no longer detectable and that it is most intense where the CH band has its greatest density:

TABLE IV

LOCATION OF COMBUSTION ZONE ACCORDING TO CH AND CO + O EMISSION WITH LONGITUDINAL OSCILLATION: 6 x .100 (922 fps) INJECTION

Chamber Pressure Psig	End of Combustion Zone inches downstream of injector	Point of Most Intense Combustion inches downstream of injector
50	4.1	3.1
100	4.4	3.0
150	4.4	2.9

It is of interest that even with sonic injection of propellants, the gion of heat release is so close to the injector face.

We have not as yet taken UV spectra, spectra of transverse oscilla- ons and of a stably operating engine, and of the associated variations in jection velocity.

The above data suggest that spectroscopy is useful in measuring ial distribution of combustion.

If we regard the long wavelength continuum as being due to a hot tal surface in the chamber (see Section 3.5.1.2) then the photographic nsity and variation with wavelength can be used as an indication of grey dy temperature. Visual inspection of Figure 23 suggests that the ximum metal temperature (and thus gas temperature) occurs about 4 inches downstream of the injector.

5.2 Densitometric Measurements

3.5.2.1 Measurement Method

Densitometric measurements were made on the original ctrographic plate of Figure 23 using a Jarrell-Ash Microphotometer, usted to read percent transmittance above fog level. The effective slit ting was 75 microns wide and 0.5 mm long.

Measurements on each of the six spectra in Figure 23 were de as follows:

The point of lowest transmittance (highest density) on the band head was found and measured. This yielded the maximum photo- phic density of the band head due to the CH radiation plus that of the lerlying continuum. The axial position in the chamber corresponding his area of maximum density is the value listed in the last column of ble IV.

The transmittance was then measured at a point in the tinuum 2 mm (on the plate) towards the red (roughly 4370A), and at same vertical position where CH band transmittance was lowest. ile the intensity of the continuum in the 4370A region is somewhat er than at 4315A, this point was selected as the closest one to the band d which appeared free of photographic edge effects and contributions m other emitters.

Because all spectra were on the same plate and given the same exposure times, the densitometric requirements of identity in emulsion, exposure time and development are met. Therefore density relationships between spectra are quantitative, even though a sensitometric plate calibration was not made as would be needed for absolute rather than relative measurement.

Except possibly for the continuum image at 50 psig, the spectra are recorded on the linear part of the sensitometric curve. More specifically, the region around 4315A is not overexposed, and the continuum not seriously underexposed, so that density values can be interpreted as being linear with the logarithm of relative exposure, or illumination at the plate.

In Figure 25 are plotted maximum density at the CH band head, density of the continuum, and density due to CH only, all versus chamber pressure. Density due to CH was computed as the difference between total density at the band head and adjacent continuum density.

In the plotted data the effect of spectrograph slit width on photographic density is as expected. Densities of the continuum, and of the CH band plus continuum differ by 0.3 to 0.5 units between the 100μ and 200μ slit exposures, as should be for continuum density or line-plus-continuum regions. Densities due to CH alone vary little with slit width, which is the expected approximation to spectral line behavior.

3.5.2.2 Effect of Pressure Upon Emission

To be noted is that continuum emission increases, while CH emission decreases with pressure, so that at 150 psig, the continuum contribution in the 4315 region is at least as great as that of CH emission.

Of particular interest is the effect of pressure on the CH emission. It should first be pointed out that the intensity of CH emission from the chamber gases is directly proportional to the number of CH emitters present, since CH at 4315A shows no self absorption in a flame or reaction zone (ref. 5, 9) and there is no extinction or scattering by carbon (Section 3.5.2). Therefore the 0.2 density unit average decrease in CH emission (Fig. 25) means that the absolute number of emitters at 150 psig has decreased to about 0.7 the number present at 50 psig, in spite of a three fold increase in gas density. Thus the concentration of excited CH at 150 psig is about 0.7/3, or about 0.23 the concentration existing at 50 psi.

This weakening of CH emission at high pressure was reported for laboratory flames in reference (7).

3.6 High Speed Motion Pictures

With the Plexiglas chamber in place (Fig. 3) Fastax movies were taken at various speeds from 2000 to 8000 frames per second. All runs with 6-port injection were underexposed because of the clean, low luminosity combustion of the premixed system.

Some runs with 12-port injection gave well exposed films. This is most likely because injection near the Plexiglas wall gave some opportunity for propellant-Plexiglas reaction with the consequent diffusion flame yellow carbon emission.

The results were of minor interest. It was revealed that for subsonic 2 x .125 (297 fps) injection at 130 psig, in the presence of audible screaming, that there were violent pulsations in the chamber, including flow reversal at times.

An attempt was made to photograph the chamber gas behavior with a radation of injection velocities: 6 x .200 (230 fps), 6 x .125 (594 fps) nd 6 x .100 (922 fps). The intent was to visualize the effect of non scillating operation, longitudinal oscillation with pressure coupling hrough the injector, and longitudinal oscillation with acoustic isolation. hese films however were underexposed as mentioned above.

Movies represented a small effort, less than fifteen runs being hotographed.

4. DISCUSSION

4. 1 General

During the course of this first year of investigation, a number of engine hardware modifications were made in order to arrive at a configuration that oscillated in the longitudinal mode and with which the desired pressure and light measurements could be made. In this evolution, we acquired many pressure measurements which were not accompanied by light measurements; good light fluctuation measurements began to be obtained towards the end of this period.

As a consequence, a fair amount of information was obtained (as indicated in Section 3) on how geometry and construction can affect combustion oscillations in a gas fed premix engine. The main interest however was in the pressure-emission fluctuation relationship, and not in the methodical study of how engine design affects the occurrence of oscillations per se. For this reason, the full range of O/F variation and chamber pressure variation was not made for most of the configurations evaluated.

In the discussion to follow, our experiences on the design-oscillation relation will be briefly commented on, to be followed by a more detailed consideration of the emission results.

4. 2 The Occurrence of Oscillations

Because our main interest is in pressure-emission relationships, we do not wish to discuss the design-oscillation relationship in any detail. In fact, for reasons stated in Section 4. 1, our data is not comprehensive enough to compare critically our results on the latter point with those of Purdue (ref 1, 3)* and Princeton (ref 2).

Purdue has already showed (ref 1, 3,10) that injection pattern markedly influences the occurrence of oscillations. Our results show that injection velocity is another strong factor in determining their occurrence. In fact,

---

*Purdue has an extensive and interesting series of reports on this topic, reporting upon both premixed and unmixed gas-fed engines. It would serve no purpose here, however, to refer to all of them.

ith 12 x .070 (943 fps) sonic injection, all operating points tested showed efinite oscillations (Section 3. 1 and Figure 12). This is quite distinct from ie results typically obtained at Purdue with subsonic injection, where specially at lower chamber pressures instability was a strong function of /F ratio. This difference applies to both the longitudinal oscillations and ie tangential oscillations (Figure 12; refs 1, 10).

Our results with the transverse modes cannot however be directly mpared to Purdue's because of their larger diameter chamber (and thus wer frequency), and different fuel (ethylene at Purdue) which will affect e pressure-kinetic interaction.

Our main point is that we believe sonic injection is necessary to couple the chamber from the feed system to be sure that the oscillations e as nearly as possible associated with perturbations in combustion, and t complicated by superimposed effects due to fluctuations in mass flow te. On this point, our data on pressure and light fluctuations (Sections 1, 3. 2, 3. 4) are not fine enough to assess the magnitude of feed coupling fects on oscillation, but the existence of an effect is qualitatively dicated.

It is not to be interpreted that sonic injection velocity per se affects the cidence of oscillation. We are more inclined to the interpretation that bsonic injection, by allowing pressure propagation through the injector, sipates some of the energy from the incident pressure wave and degrades intensity of the pressure-combustion interactions.

3 The Phasing of Pressure and Emission Fluctuations

As noted in Section 3. 4. 1, no light fluctuations were observed which re associated with transverse pressure oscillations.

Longitudinal oscillations however were always accompanied by ctuations of the same frequency in the CH and OH band emission and in the al luminosity. Referring to the pressure-emission time lags in the last umn of Table III, it is seen that the lags for subsonic injection are not ferent from those for sonic injection. Thus, except for the fact that there differences in the shape of the light traces (Section 3. 4. 2. 1), these data not reveal any differences in the pressure-heat release relationship that ght result from an oscillation-mass feed rate interaction.

For sonic injection there is a small but clear and regular lag with respect to pressure of the OH and CH emission traces at 50 psig and 100 psig, but no lag at 150 psig chamber pressure. It is not certain that the differences in the tabulated time lags (Table III) between OH and CH at a single pressure, or between 50 and 100 psig chamber pressure are significant owing to the estimated uncertainty of 0.1 millisecond in reading the time from the records. It is however considered that the zero lags tabulated for OH and CH at 150 psig, and for the total luminosity at 50 and 100 psig, represent a real difference from the finite lags noted above.

From the measured flame thickness and burning velocity for stoichiometric premixed methane-air at one atmosphere, .0137 cm (ref 11) and 35 cm sec^{-1} (ref 12) respectively, one can estimate a reaction time of 3.9×10^{-4} seconds (.39 ms) for complete conversion of reactants to products.

On the basis that, for a bimolecular kinetic system such as methane-air, reaction time for an elemental mass of reactant varies as 1/pressure*, the total reaction time can be extrapolated to higher pressures. This is showed in Table V.

TABLE V

ESTIMATED REACTION TIME FOR STOICHIOMETRIC METHANE-AIR AT VARIOUS PRESSURES

Pressure, psig	Pressure, psia	Reaction Time milliseconds
0	15	.39
50	65	.09
100	115	.05
150	165	.04

*Bimolecular rate, $\frac{\text{mols}}{\text{sec cm}^3} \propto p^2$

Since $\frac{1}{\text{cm}^3} \propto p$, $\frac{\text{mols}}{\text{sec}} \times p \propto p^2$

and $\frac{\text{mols}}{\text{sec}} \propto p$; and $\frac{\text{sec}}{\text{mol}} \propto \frac{1}{p}$

Although the time lags listed in Table III for the OH and CH emission at e three pressures are not numerically the same as the estimated total action times, they are of similar value and have an apparently similar essure dependence. This suggests, although perhaps inconclusively, that e radical emission fluctuations do indeed reflect an interaction between essure and the early chain branching phases of the combustion reaction.

In contrast, the in-phase property of the total luminosity (CO + O ntinuum) record with respect to the pressure suggests that the emission ictuations here are due to some more direct effect of pressure upon issivity or the CO + O reaction itself and not to changes in the rate of e chain branching reactions.

4 Interaction of Pressure and Emission Fluctuations

4.1 Experimental Values for Pressure Exponent of Emission

A measure of the interaction between the pressure fluctuations and e emission fluctuations can be obtained from the amplitude data in ble III through the relationship

$$\frac{E_{max}}{E_{min}} = \left(\frac{P_{c_{max}}}{P_{c_{min}}}\right)^n$$

E_{max} = Maximum emission value, mv

E_{min} = Minimum emission value, mv

$P_{c_{max}}$ = Maximum chamber pressure, psia

$P_{c_{min}}$ = Minimum chamber pressure, psia

n = Pressure exponent of emission

Data for sonic injection, stoichiometric conditions (see Table III a of Figures 20-22) when so treated and evaluated for the pressure onent, n, yield the values listed in Table VI.

TABLE VI

PRESSURE EXPONENT OF EMISSION
UNDER LONGITUDINAL OSCILLATING CONDITIONS

Band	Chamber Pressure psia	$\frac{P_{c_{max}}}{P_{c_{min}}}$	$\frac{E_{max}}{E_{min}}$	Pressure Exponent n
OH	65	1.1	1.27	2.6
	115	1.19	1.31	1.55
	165	1.2	1.29	1.4
CH	65	1.17	1.5	2.65
	115	1.19	2.0	4
	165	1.2	3.0	6
Total Luminosity	65	1.13	1.65	4.1
	115	1.19	2.0	4

The response of emission to pressure oscillations with regard to chamber pressure level is different for the three emission bands:

OH: n decreases from 2.6 at 65 psia to 1.4 at 165 psia
CH: n increases from 2.65 at 65 psia to 6 at 165 psia
Total: n has a constant value of 4 at 65 and 115 psia

For comparison with these values and trends, estimates can be made of the values of n if the increase of emission with pressure were due not to reaction kinetic effects but the following mechanisms:

(a) Purely gas density effects. That is, if the gas density varies with pressure and there are no changes in composition due to chemical reaction, the concentration of the emitter in both the excited and ground state remains constant, but the absolute number varies directly with density and thus pressure.

(b) Isentropic compression--thermal excitation effects. Assuming the emitter is thermally (collision) excited, and that an isentropic temperature rise (and drop) results from the passage

of each pressure wave, the concentration of excited state emitters will rise and fall with pressure due to isentropic temperature changes in the gas.

4.2 Gas Density Effects

Because CH (4315) and the CO + O continuum do not self-absorb, the issivity for CH and total luminosity should vary directly with pressure nsity) and the pressure exponent, n, would have the value 1.0.

For OH, which does self-absorb, the Beer-Lambert law can be used stimate the pressure effect on emissivity ϵ_λ according to the equation:

$$\epsilon_\lambda = 1 - e^{-k_\lambda cLP}$$

re ϵ_λ emissivity at wavelength λ
k_λ absorption coefficient of radiation, $(cm^{-1})(atm^{-1})$
c mol fraction of absorbing species
L path length through gas, cm
P pressure, atm

Assuming an OH mol fraction of 0.02 and a k_λ of 0.1, emissivities the gas in our 3-inch i.d. chamber (7.5 cm) are estimated to be:

$$\text{for } P_c = 65 \text{ psia, } \epsilon_\lambda \approx .06 \text{ and } \frac{d\epsilon_\lambda}{dP} \approx .014 \text{ atm}^{-1}$$

$$\text{for } P_c = 165 \text{ psia, } \epsilon_\lambda \approx .13 \text{ and } \frac{d\epsilon_\lambda}{dP} \approx .013 \text{ atm}^{-1}$$

The OH radiation is thus estimated to behave as though the source e optically thin ($\epsilon_\lambda << 1$) where the emissivity is approximately portional to pressure, and the pressure exponent of emission, n, would roach unity.

There is increased optical thickness at 11 atmospheres (150 psig). e above numerical estimates are too low, the real optical thickness ld be significant, and the pressure coefficient, n, would be less than y.

4.4.3 Thermal Excitation Effects

For thermally excited emitters,* the excited state population with respect to the ground state population can be estimated from the equation

$$\frac{N^*}{N_o} = ae^{-E/kT}$$

where N^* number of the species in the excited state
N_o number of the species in the ground state
a proportionality constant
E energy of transition, ground to excited state
k Boltzmann's constant
T temperature °K.

We now assume that the temperature of the gases respond isentropically to pressure fluctuations, according to the equation

$$\frac{T_{max}}{T_{min}} = \left(\frac{P_{c_{max}}}{P_{c_{min}}}\right)^{\frac{\gamma - 1}{\gamma}}$$

where

$\frac{P_{c_{max}}}{P_{c_{min}}}$ ratio of peak to minimum pressure

$\frac{T_{max}}{T_{min}}$ ratio of gas temperatures which correspond to the above pressure extremes

γ ratio of specific heats

From the pressure ratio data in Table VI for the OH emission,** a gas temperature ratio can be calculated, which, when introduced into the

*i.e., the excited state population maintained by collision process, not by chemical reaction or shift in equilibrium ground state population.

**This estimate cannot be applied to the CH and CO + O (Total Luminosity) data since the excitation for these emitters is by chemical reaction and not thermal collision processes.

hermal excitation equation, will yield the ratio:

$$\frac{\text{excited state population at } P_{max}}{\text{excited state population at } P_{min}}$$

f the chamber gases are optically thin with respect to OH (ground state), ıe emission intensity should be nearly proportional to excited population. .ccordingly, for the transition energy corresponding to the wavelength 100A, * and for an estimated chamber temperature of 2150°K, the net esult of such a calculation is that the pressure coefficient, n, would have ıe value 4. 1 for all three chamber pressures for OH band emission.

. 4. 4 On the Excitation Mechanisms during Oscillation

The experimental data on the pressure exponent of emission ection 4. 4. 1) and on the pressure-emission phase relationships ection 4. 3) give a basis for tentative assignment of the mechanisms of ressure-emission interactions, when considered in conjunction with the regoing theoretically considered mechanisms. For all three emission ands, the experimental pressure exponent, n, being greater than unity recludes these fluctuations being associated with density effects alone ection 4. 3. 2). This mechanism will not be further considered. Other spects are discussed below.

OH Emission Fluctuations. A thermal excitation mechanism ssociated with isentropic compression heating (Section 4. 4. 3) could account r the OH fluctuations. The theoretical pressure exponent for this echanism, 4, is well in excess of the experimental values.

On the other hand, a kinetic mechanism is also consistent with the perimental data. The elementary reactions that form the OH radical e bimolecular, such as

$$CH_4 + O = CH_3 + OH$$

$$CH + O_2 = CO + OH.$$

ıe bimolecular pressure exponent, n = 2, is clearly compatible with perimental values of 1. 4 to 2. 6.

. 4 x 10^{-12} erg $molecule^{-1}$ $^oK^{-1}$, or 92 kcal gm mol^{-1}

The decrease in OH pressure exponent with increasing chamber pressure level also is consistent with a kinetic mechanism. The decrease in OH emission rotational temperature with increase in pressure reported elsewhere (ref 7) is indicative of a reduced chemiluminescent contribution to OH emission* with increasing pressure. This, coupled with a possibly significant increase in optical thickness (Section 4. 4. 3) and thus self-absorption, can explain the pressure exponent behavior.

A last consideration is that the OH emission fluctuation showed a decreasing lag with respect to the pressure that was similar to the expected decrease in reaction time with increasing pressure (Section 4. 3).

The overall indication is thus that for the OH band a kinetic mechanism contributes strongly to the link between pressure and emission fluctuations, although the isentropic compression--thermal excitation mechanism may also be involved to a lesser degree.

Total Luminosity Fluctuations. The pressure-dependent excitation mechanism cannot be that of isentropic compression--thermal excitation because the origin of the continuum emission

$$CO + O \longrightarrow CO_2 + h\nu$$

is not susceptible to collision excitation. A change in this reaction resulting from changes in the rates of early reaction steps is also unlikely because of the erratic but essentially zero time lag of the total emission, compared to the definite lags for the chain branching reactions resulting in OH and CH emission in Section 4. 3.

The experimental pressure exponent of n = 4 is inconsistent with a pressure exponent of n = 2, representing the direct effect of pressure on bimolecular reaction rates. Thus the emission cannot be due to the direct effect of pressure on the CO + O reaction itself.

The present data are inadequate to make a probable assignment of interaction mechanism.

---

*Chemiluminescence for OH emission in the hydrocarbon-air reaction zone is well established.

CH Emission Fluctuations. The photomultiplier responded to the tal irradiance passed by the filter, that is to CH band emission plus a ntribution from the underlying and adjacent continuum. Nevertheless, a mparison of the pressure exponents for CH (plus continuum) and for total minosity (Table VI) indicates that the CH emission dominates the signal.

As was the case for the CO + O emission, the CH emission ictuations cannot be attributed to thermal excitation driven by isentropic mpression, since the CH (4315) excitation is non-thermal, but is due to emiluminescence according to the reaction

$$C_2 + OH = CH^* + CO.$$

This exclusion, along with the time lag in the emission and its change th pressure (Section 4. 3) suggests that the CH emission fluctuations are ked to the pressure fluctuations through the chain branching propagation actions.

A remarkable feature is the increase in pressure exponent with amber pressure level, far exceeding the value of 2 or 3 that would scribe the pressure dependence of bimolecular or even termolecular actions.

It is not profitable to attempt interpretation in terms of the effect of essure on the reactions forming the excited CH radical, as these reactions e postulated to involve reactions of the radical C_2, whose origin is not derstood (refs 13, 14). Thus for the time being we accept this behavior the CH emission during oscillations as an experimental fact subject to ssible later elucidation.

Of interest however is the positive pressure response of the CH ission during oscillation compared to the negative slope of CH radiant ensity versus chamber pressure observed in the densitometric analysis of ne-averaged photographic spectra (Section 3. 5). The two types of data nnot be directly compared because the photomultiplier signal includes sponse to the continuum as well as the CH band, although at low chamber essures this contribution appears small (Figure 25).

There is however the possibility, suggested by the shape of the) psig CH oscilloscope record (Figure 22b and Section 3. 4. 2. 1) that re is a relaxation effect in the adjustment of the CH (excited) population an increase in pressure.

We can say that the CH population is determined by a balance between reactions which form CH in the excited state and reactions which compete with its formation or which remove it, including radiation. In Figure 22b, the sequence of CH emission peak amplitude is reversed over that at lower pressures; that is, the first spike in the CH trace is larger than a subsequent spike within one period of the basic longitudinal mode oscillation. This would be consistent with an overshoot in CH population as would occur if the CH-producing reactions responded rapidly to a pressure rise, with a slower response of the CH-reducing reactions to make the final adjustment of the kinetic scheme as a whole to the new pressure.

This is of course speculative, but such an effect would account for the positive response of CH emission to pressure oscillations. It could also account for the greater pressure exponent of CH emission at elevated pressure levels, where the amplitude of the pressure oscillation is increased and thus, at constant frequency, the absolute rate of pressure change is increased.

5. IMPLICATIONS FOR THE STUDY OF OSCILLATORY COMBUSTION

5.1 General

Although the inferences which can be drawn from the data thus far obtained are qualitative or, at best, semi quantitative, they are meaningful in terms of research methods in the study of rocket oscillations. Some remarks in this regard are in the following paragraphs, with regard to the utility of light emission measurements, the processes in oscillatory combustion, and the use of gas-fed engines.

5.2 Utility of Light Emission Measurements

The OH (3064A) and CH (4315A) emission are reliable indicators of a change in the rate of the chain branching steps of the combustion reaction resulting from the passage of a pressure wave.

The OH emission may be useful only for relatively low pressure levels as its response to pressure pulses falls as pressure level is increased. This may be because of a reduction in chemiluminescent contribution to total OH emission. This would also mean that the radiation becomes less uniquely representative of the reaction zone, since OH is also a stable combustion product and susceptible to thermal excitation. If spectrograms of the UV radiation from the engine become available this point may be clarified. Another limitation will be found as engine size is increased or as higher temperature reactions (i.e. hydrocarbon-oxygen, hydrogen-oxygen) are studied as both will increase the ground state OH population and the resultant self-absorption, reducing the pressure response of the OH radiation. *

The CH emission has the attractive features of emanating only from the reaction zone and of being without self-absorption at 4315 except for extremely long paths. The pressure response of CH radiation should therefore be observable even in rather large engines, subject to limitations arising from strong background radiation.

---

*Ref. 15 indicates emissivities of OH radiation from H_2-O_2 combustion products, for a path length of 2-4 inches, to be as high as .580 at 300 psi.

It would seem, both from our spectrograms and from the more extensive set in ref 7 , that for hydrocarbon-air premixed and diffusion flames at elevated pressures the CH radiation becomes so suppressed with respect to the background that it would become useless as an indicator of reaction rate. This becomes more pronounced for hydrocarbon-oxygen flames. However these spectra are time-averaged, and our high frequency data seem to indicate that for transient conditions the readability of the CH emission may extend to higher pressure levels than implied by the time-averaged spectra.

In summary, these light fluctuation measurements may not be usable with large engines using high temperature propellant systems at 20 atmospheres chamber pressure, but as research measurements on a smaller scale, or "sliced section" engines, etc., may be generally feasible.

5.3 Relation of Chemical Kinetics to Oscillatory Combustion

It is evident from our records that even in the case of the kinetically sluggish methane-air system, the combustion response to a low-amplitude (say 20%) pressure wave is complete within 200 microseconds (or less) at 50 psig and in tens of microseconds at 150 psig.

These reaction times are short with respect to the period of the 1000-1200 cps longitudinal oscillation (about 800 to 1000 μ s) but are of the same order as the periods for the 7100 and 14,000 cps transverse modes (140 μ s and 70 μ s). Therefore if the criterion for combustion-driven oscillations is a small phase angle between pressure and heat release oscillations, the 1000 cps mode should always be driven, while the 7100 and 14,000 cps modes could either be driven or damped depending upon the precise combustion response time. It is not clear from our data whether there was any real trend in the transverse oscillations vs pressure and O/F which could be related to this notion. If in the future we are successful in getting light measurements at an aspect angle of 90° to the direction of transverse wave propagation* we can comment more pointedly on this matter.

---

*That is, a line of sight parallel to the engine axis.

It is however clear that for real engines, where dimensions are large* and fast burning propellants are used, oscillation periods will be large (order of 1 ms or greater) compared to reaction times which would be on the order of 10μs or less. Thus some process having a relatively slow pressure response, about half the oscillation period, would be needed to decouple the heat release from the pressure fluctuation. Such processes are of course to be found in the physical rates of atomization, vaporization, and mixing.

This is certainly not a new thought as the rate controlling nature of these physical processes have been repeatedly pointed out by others. However, our data seem to us to give experimental confirmation of the fast response of chemical kinetics to pressure fluctuations. Further, the observation of emission as we have described would in our opinion be valuable to measure the magnitude of the rates of these physical processes with liquid propellants.

5.4 The Gas-Fed Engine as a Research Device. The intent here is neither to praise nor condemn the gas fed engine, but to express our thoughts, after a year's acquaintance with one, as to its place in research on oscillatory combustion.

Firstly, to the extent that reaction kinetics are pertinent, it is useful. Measurements of reaction response to transient pressure as reported herein are made possible and are useful. It can be valuable in studying, with suitable reactants, high-pressure emission or absorption spectra; it has been instructive that spectra from laboratory flames appear to have corresponding spectra when the reactants are burned under rocket conditions.

Secondly, an oscillating gas fed engine may be useful to study the departure from steady state behavior of a complicated kinetic scheme under transient pressure change. This now is concerned with fully developed combustion, and not ignition which is readily adaptable to shock tube experiments. In this respect attention is invited to the surprising behavior of CH emission burning oscillation.

Small space-vehicle engines such as verniers may thus be excluded from the following remarks.

One thing the gas-fed engine will not do is to represent a laboratory model of real-life rocket oscillation, as two of the real-life processes which are designed out, atomization and vaporization, have pressure response rates of the right order to be critical in determining the stability of a rocket chamber. Nevertheless, an engine capable of operating on gas reactants as one mode of operation appears useful in establishing comparison base lines and experimentally separating variables.

6. REFERENCES

J. R. Osborn and R. L. Derr, An Experimental Investigation of Longitudinal Combustion Pressure Oscillations. Purdue Univ. Report No. I-62-8, Aug. 1962, Contract Nonr 1100(21).

R. Pelmas, I. Glassman, and M. Webb, An Experimental Investigation of Longitudinal Combustion Instability in a Rocket Motor using Premixed Gaseous Propellants. Princeton Univ. Report No. 589, Dec. 1961, Contract AF 62-90.

J. R. Osborn and A. C. Pinchak, Investigation of Aerothermodynamic Interaction Phenomena in Combustion Pressure Oscillations. Purdue Univ. Report No. I-59-2, June 1959, Contract N7onr 39418.

(Deleted.)

R. G. W. Norrish, G. Porter, and B. A. Thrush, Studies of the Explosive Combustion of Hydrocarbons by Kinetic Spectroscopy. I. Free Radical Absorption Spectra in Acetylene Combustion. Proc. Roy. Soc. A216, 165, 1953.

A. G. Gaydon, The Spectroscopy of Flames. Wiley (New York), 1957.

J. Diederichsen and H. G. Wolfhard, Spectroscopic Examination of Gaseous Flames at High Pressure. Proc. Roy. Soc. A236, 89 (1956).

B. Hornstein, Research Study of Light Emission Caused by Pressure Fluctuations in Rocket Motors. Reaction Motors Report No. RMD 5516-SA1, July 1964, Contract AF 49(638)-1279.

A. G. Gaydon, G. N. Spokes, and J. van Suchtelen, Absorption Spectra of Low Pressure Flames. Proc. Roy. Soc. A256, 323.

J. R. Osborn and J. R. Rahon, Effects of Radial Energy Release Variations on Transverse Combustion Pressure Oscillations. Purdue Univ. Report No. I-62-3, March 1962, Contract Nonr 1100(21).

K. Wohl, in Fourth Symposium on Combustion, p. 48. Williams and Wilkins (Baltimore) 1953.

REFERENCES (Continued)

12. B. Lewis and G. von Elbe, Combustion, Flames and Explosions of Gases, Academic Press (New York), 2nd Ed. 1961.

13. A. G. Gaydon and H. G. Wolfhard, in Fourth Symposium on Combustion, p. 211, Williams and Wilkins (Baltimore), 1952.

14. G. B. Kistiakowsky, J. V. Michael, and H. Niki, The Oxidation Reactions of Acetylene and Methane. Preprinted for the Tenth Symposium on Combustion (1964).

15. M. C. Burrows and L. A. Povinelli, Emission Spectra from High Pressure Hydrogen-Oxygen Combustion. NASA TN D-1305, July 1962.

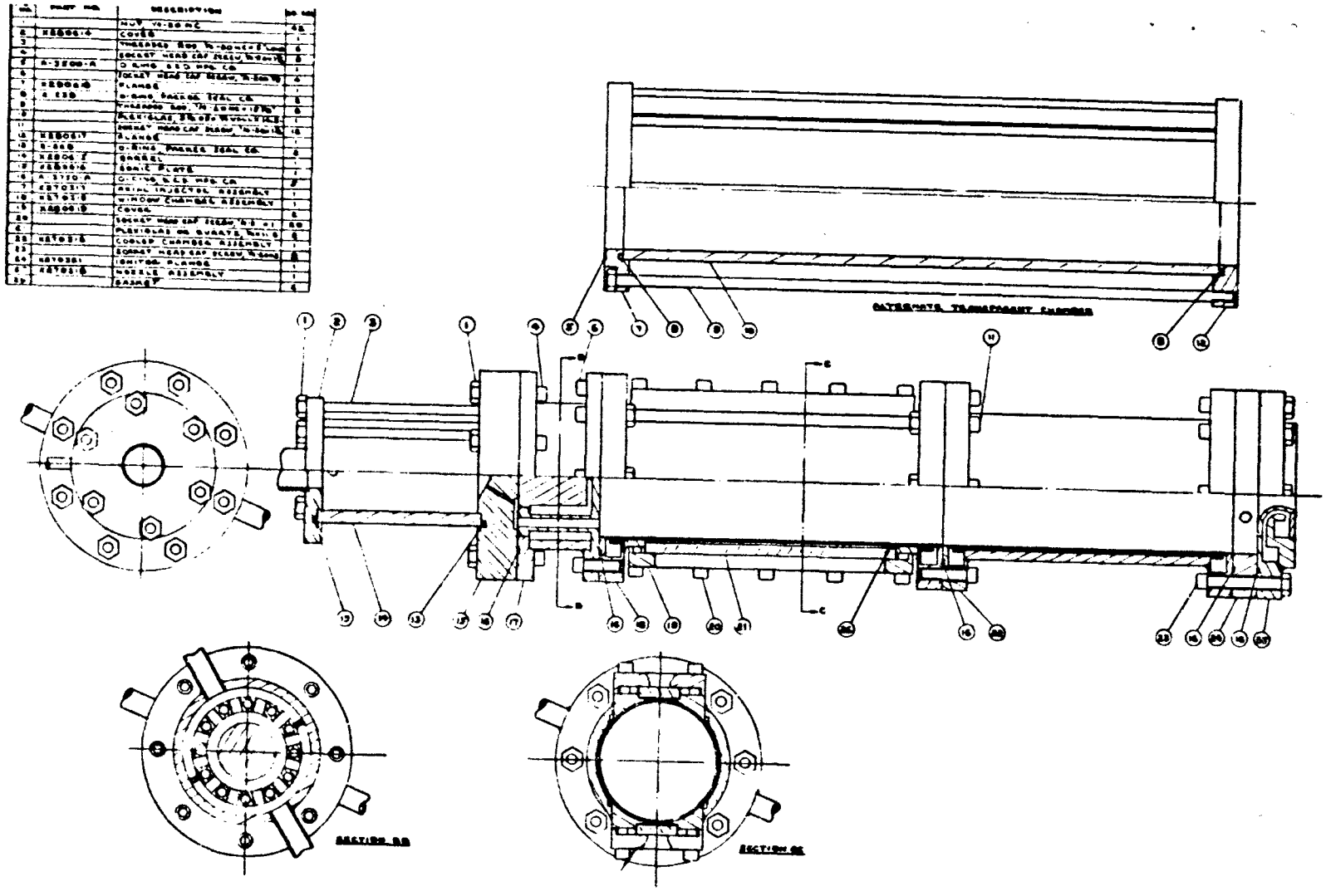

RMD Drawing No. X265030

Fig. 1. Assembly Drawing of Engine, Showing Water-Cooled 12-Port Injector, Water-Cooled Metal Chamber, and Plexiglas Chamber.

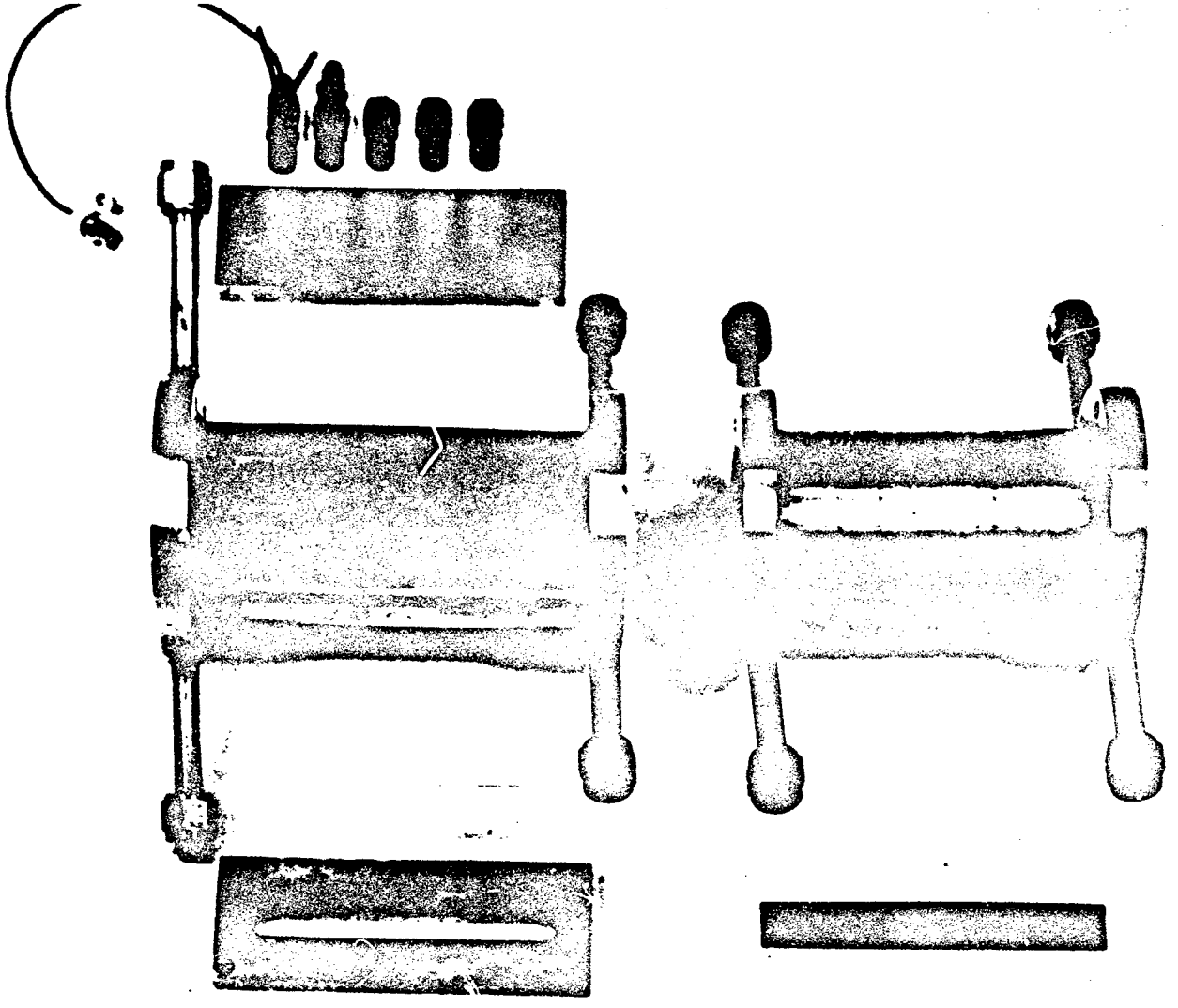

RMD Photo No. 5520-1

Fig. 2. Water-Cooled Chamber, Showing (above) Pressure Tap Plate with Two Pressure Fittings and 3 Blank Plugs, and (below) Quartz Window and Retainer.

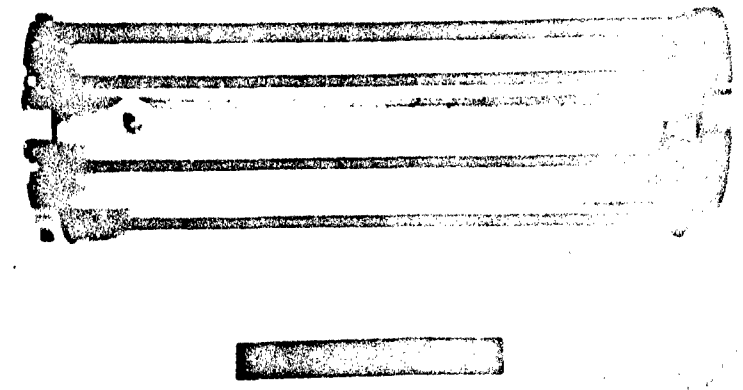

RMD Photo No. 5520-4

Fig. 3. Plexiglas Chamber Assembly.

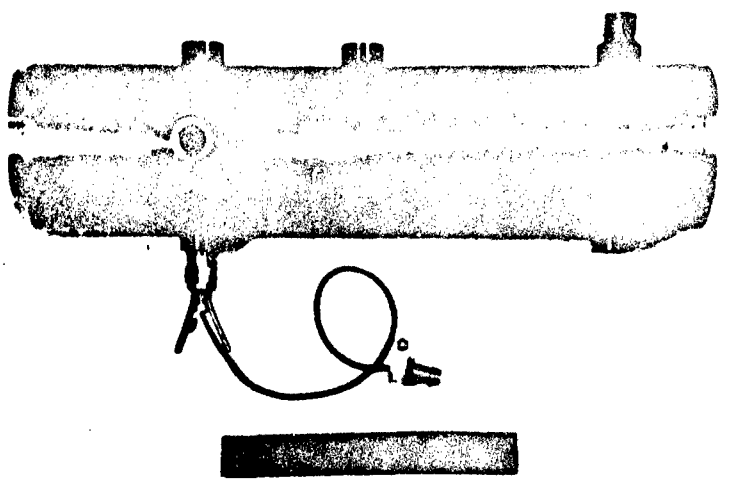

RMD Photo No. 5520-3

Fig. 4. Uncooled Metal Chamber Barrel, with Kistler Assembly and Blank Plug.

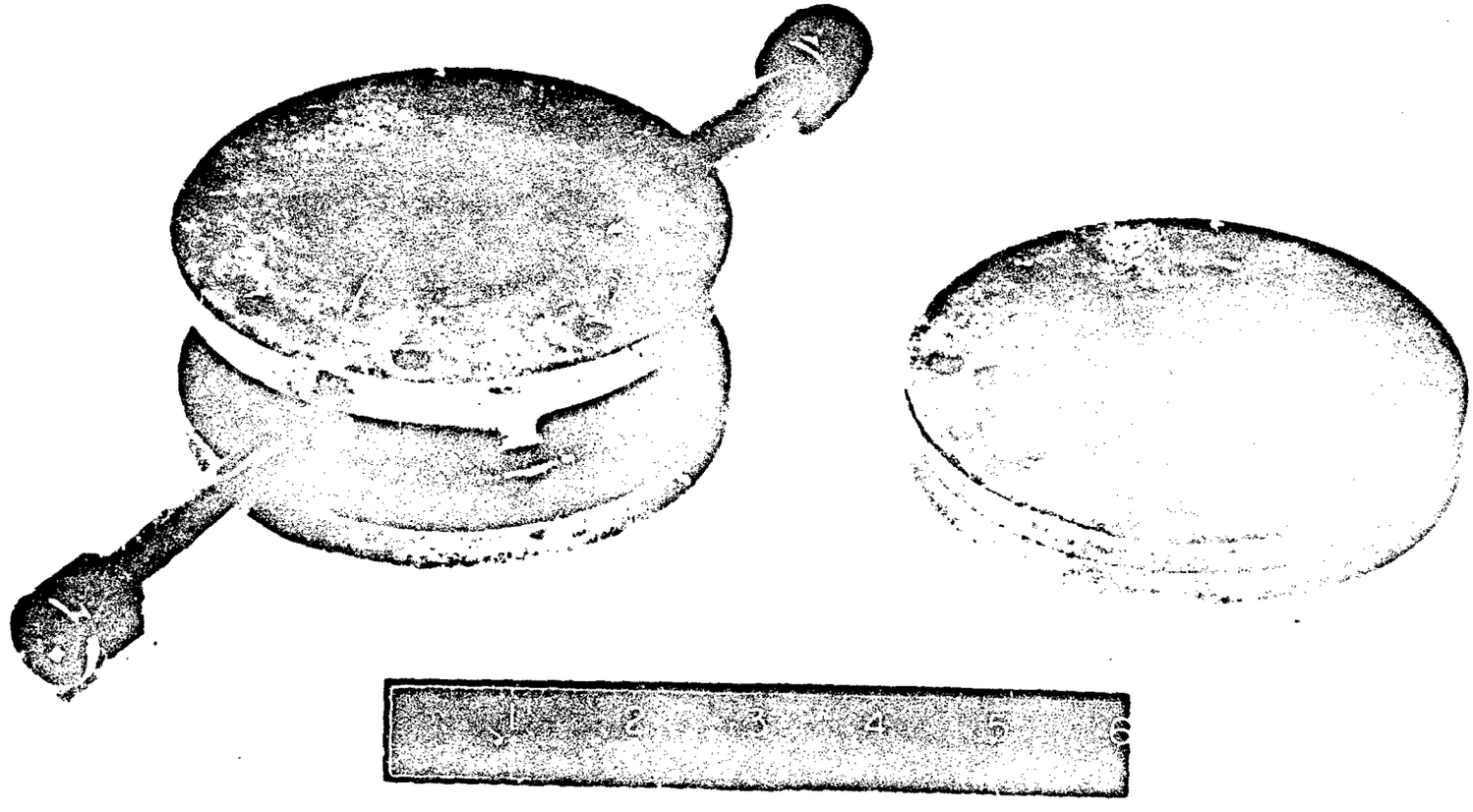

RMD Photo No. 5520-5

Fig. 5. Water-Cooled 12-Port Injector and Uncooled 6-Port Injector, Showing One Insert Partially Screwed in.

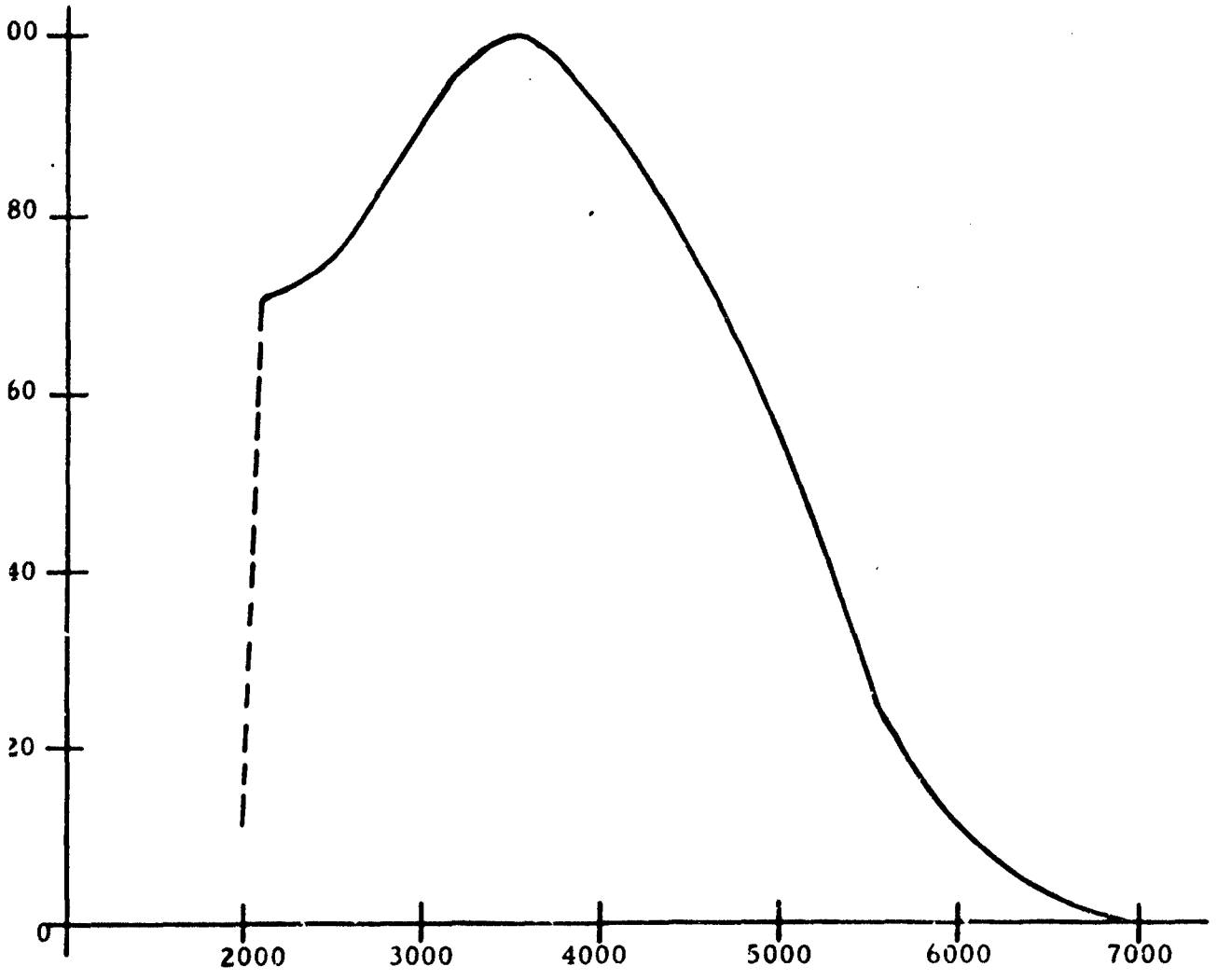

Fig. 6. Spectral Response of RCA
Type 1P28 Photomultiplier Tube

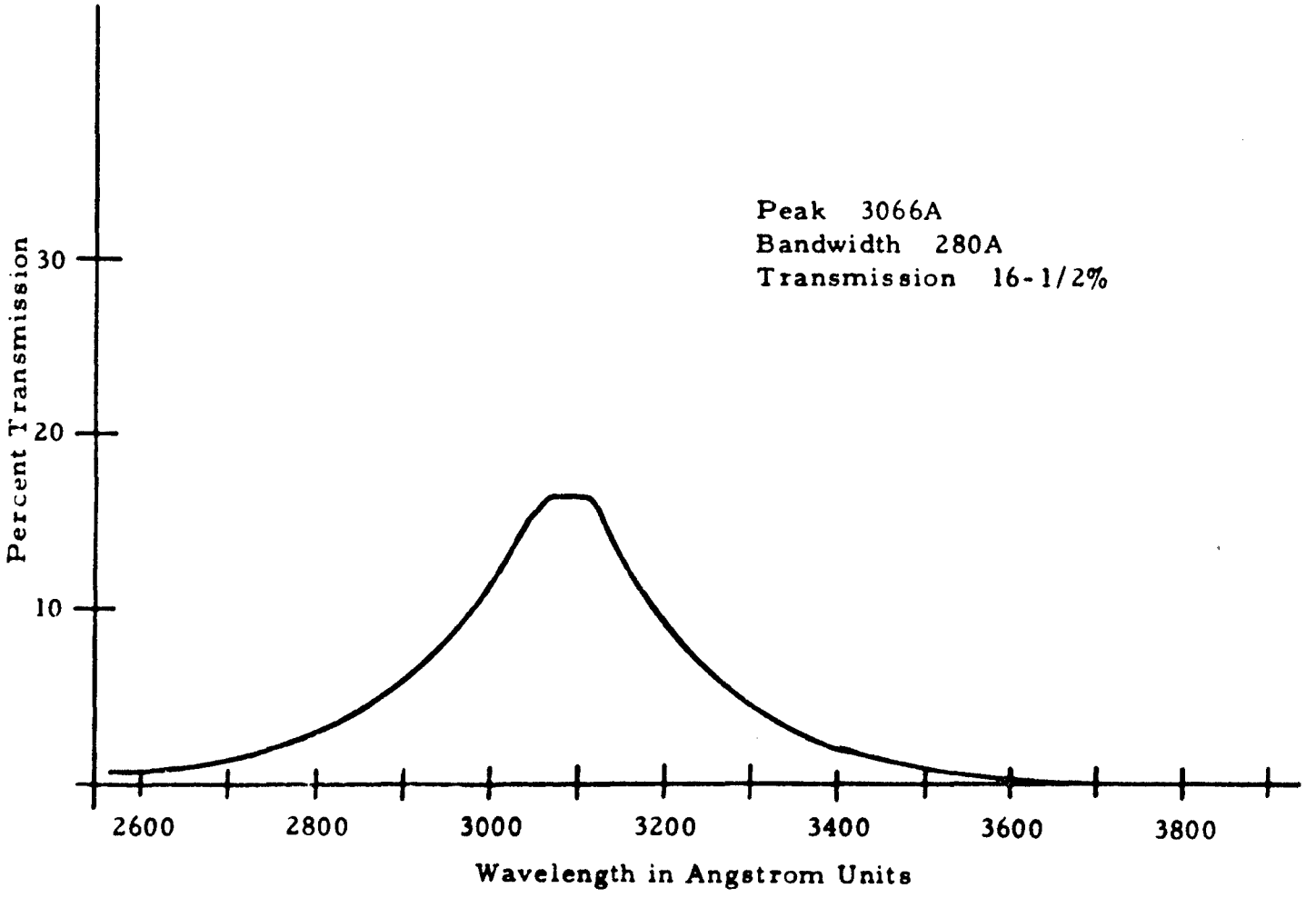

Fig. 7. Transmission of Baird Atomic Interference Filter for the OH (0, 0) Band at 3064A.

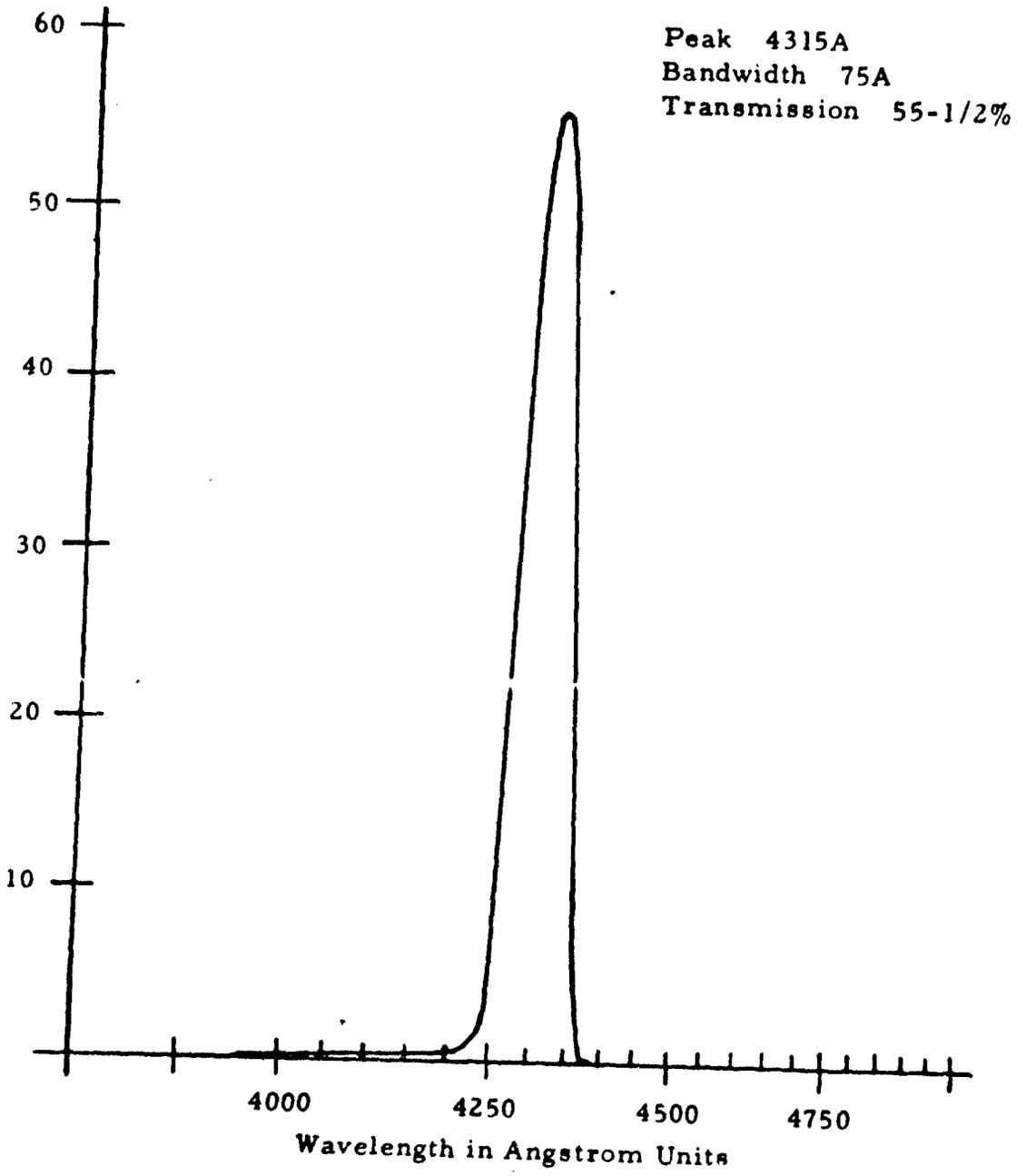

Fig. 8. Transmission of Baird Atomic Interference Filter for the CH (0, 0) Band at 4315A

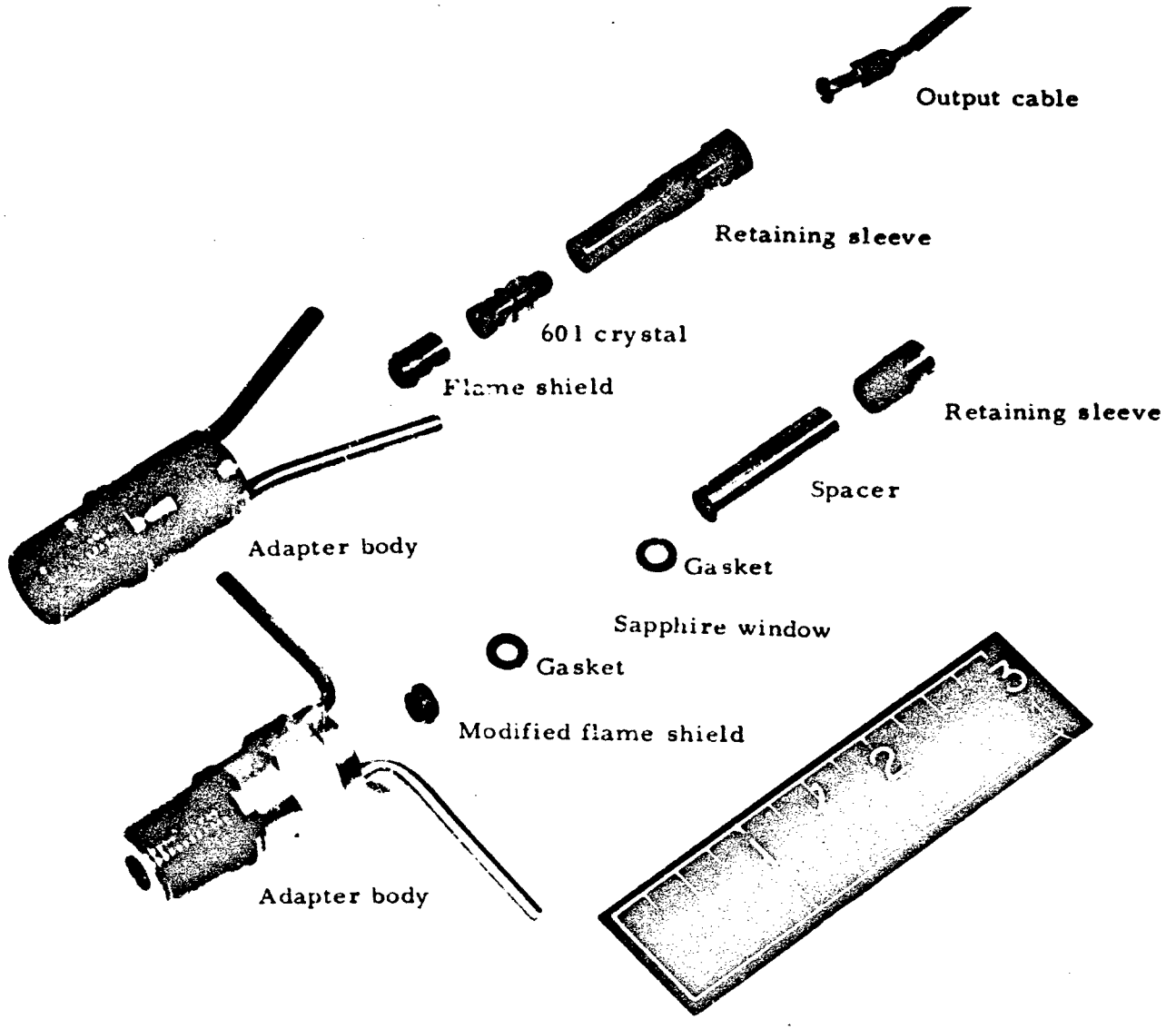

RMD Photo No. 5520-2

Fig. 9. Kistler Water Cooled Adapter and Crystal Unmodified (above), and Modified as Sapphire Window Assembly (below).

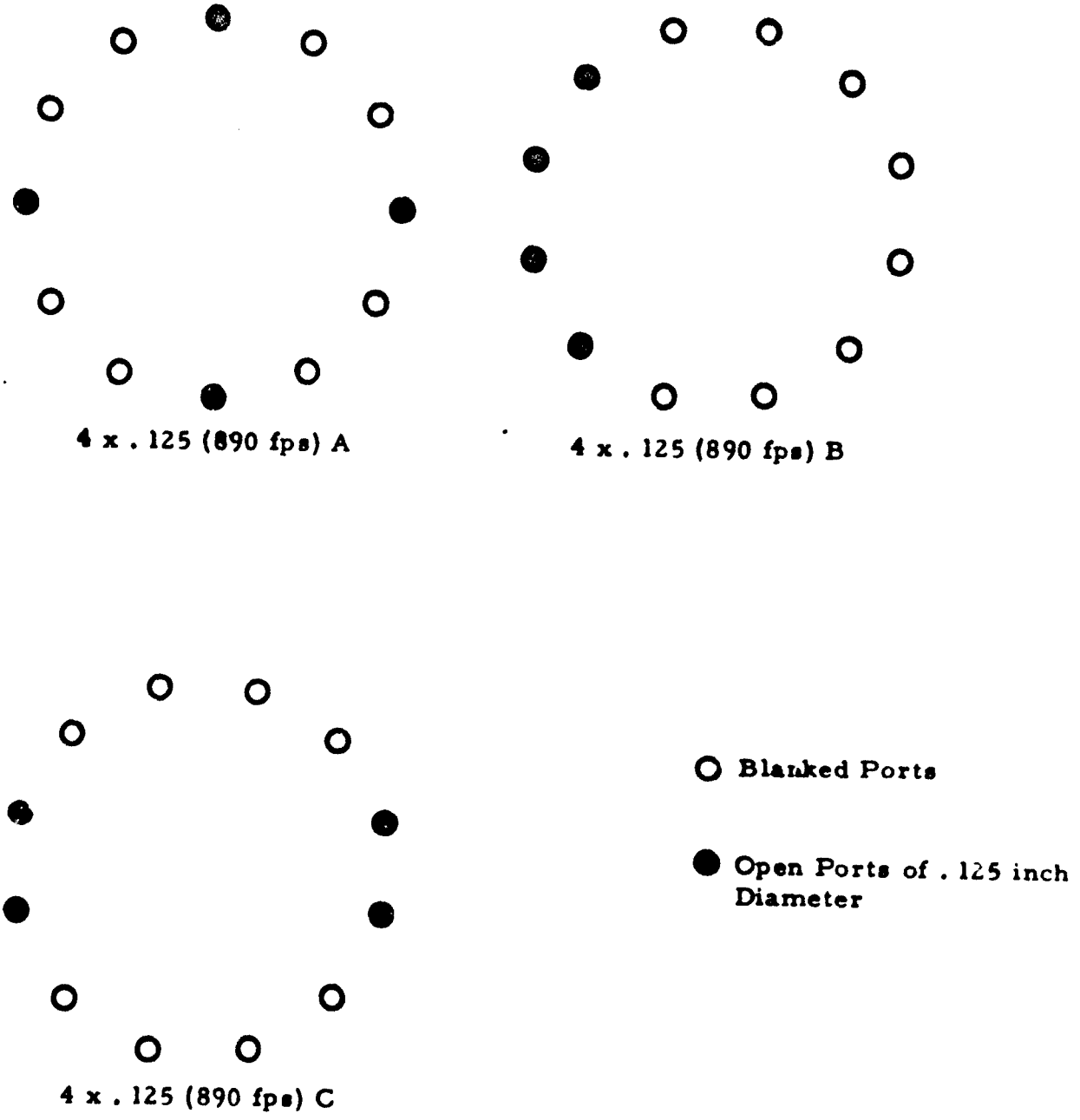

Fig. 10. Injector Patterns for 4 x . 125 (890 fps) Injection.

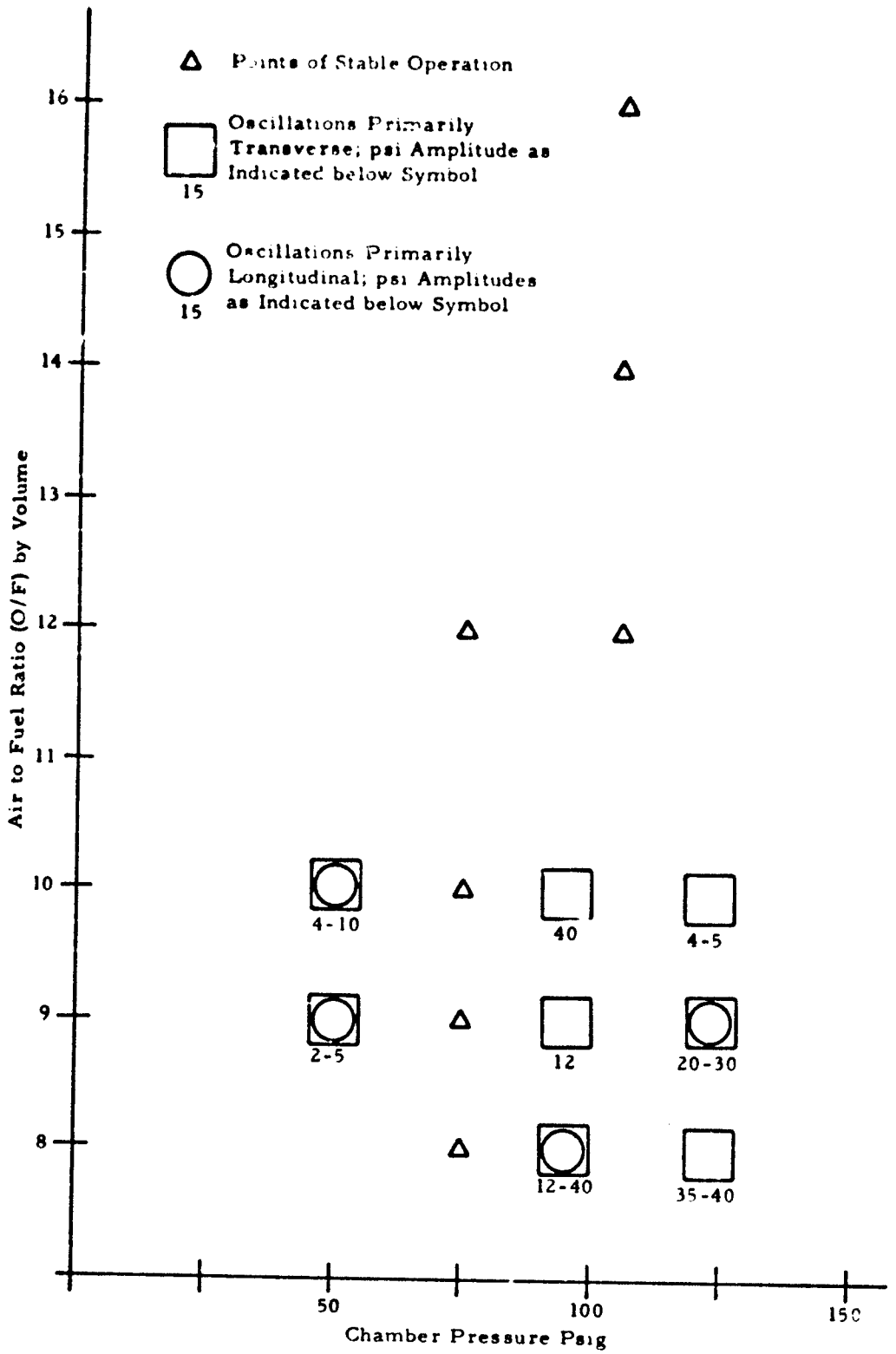

Fig. 11. Incidence of Pressure Oscillations with 11 x .125 (333 fps) Injection; Uncooled Metal Chamber.

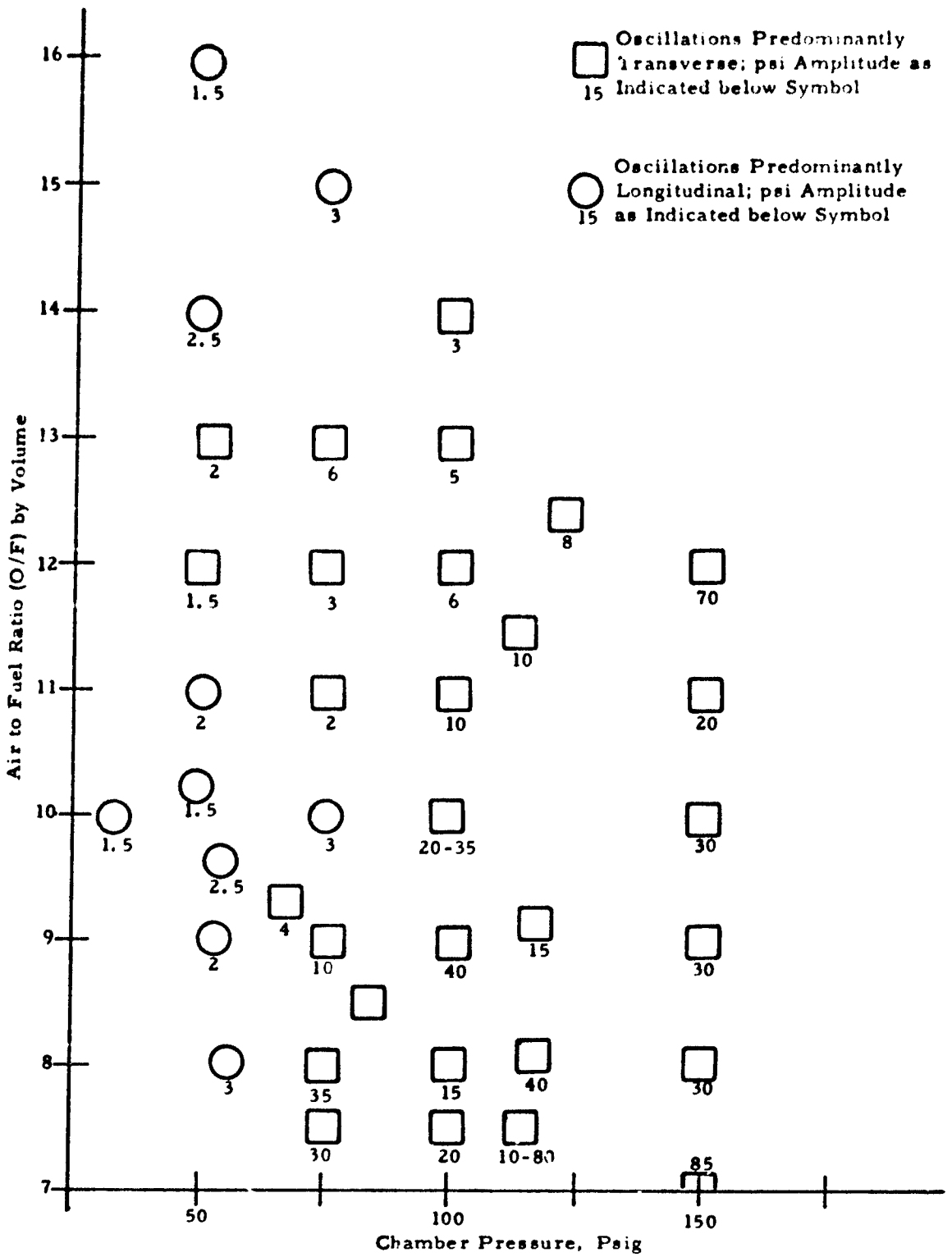

Fig. 12. Incidence of Pressure Oscillations with 12 x .070 (943 fps) Injection; Uncooled Metal Chamber.

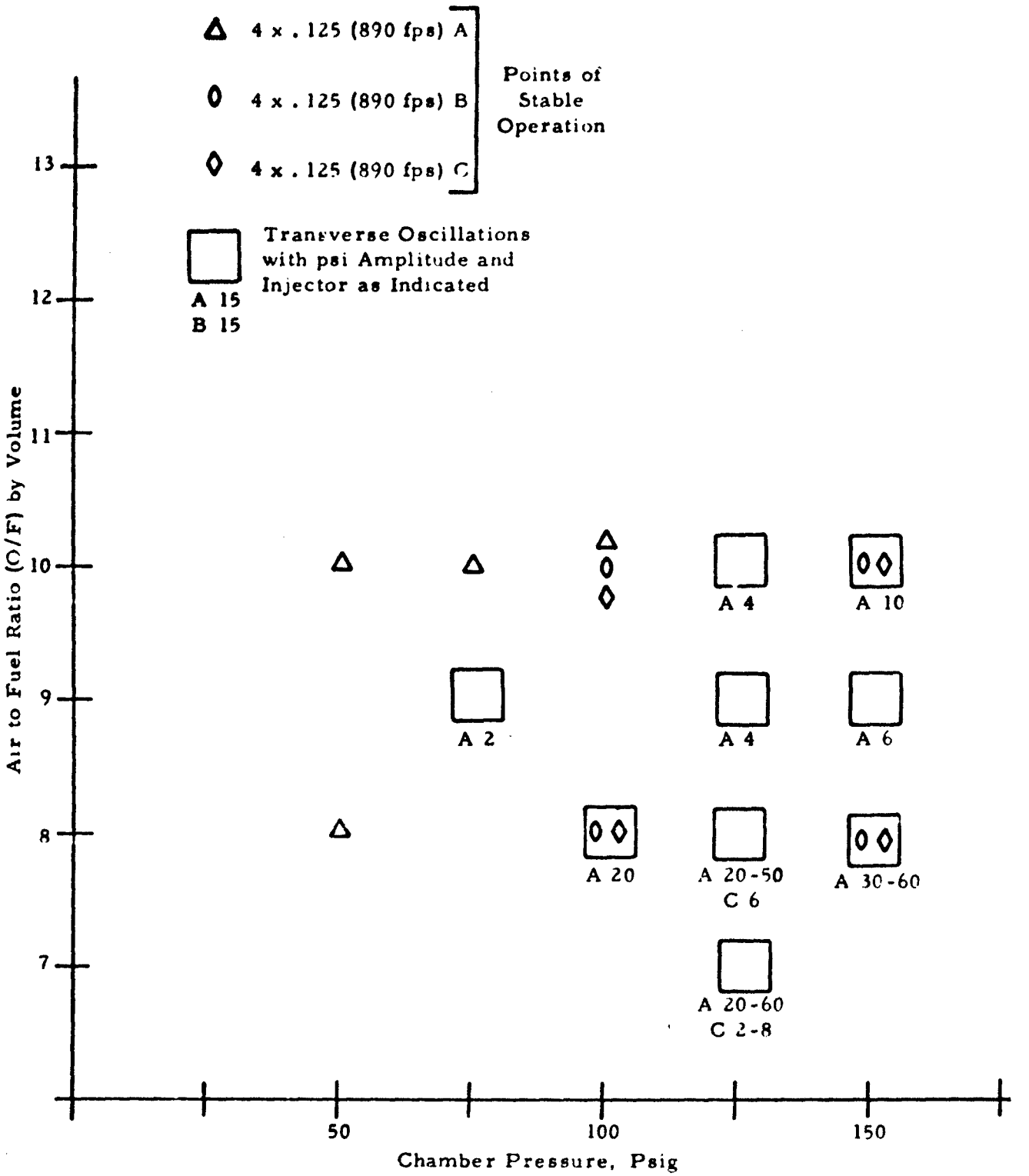

Fig. 13. Incidence of Pressure Oscillations with 4 x . 125 (890 fps) Injection; Uncooled Metal Chamber.

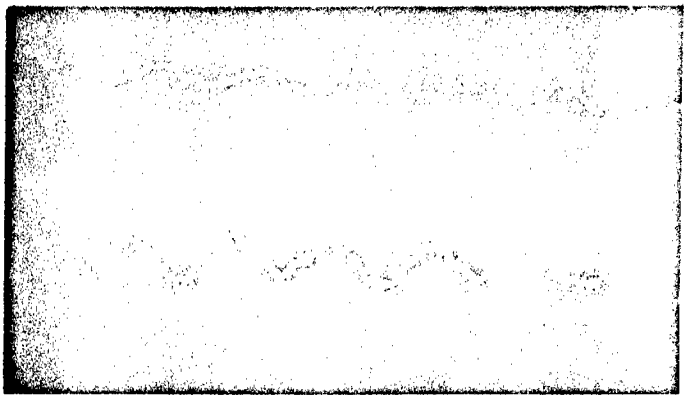

P_c = 100 psig; O/F = 8

Upper, P_c = 5 psi/div

Lower, P_i = 5 psi/div

Time = .5 ms/div

(a) 6 x .200 (290 fps) injection

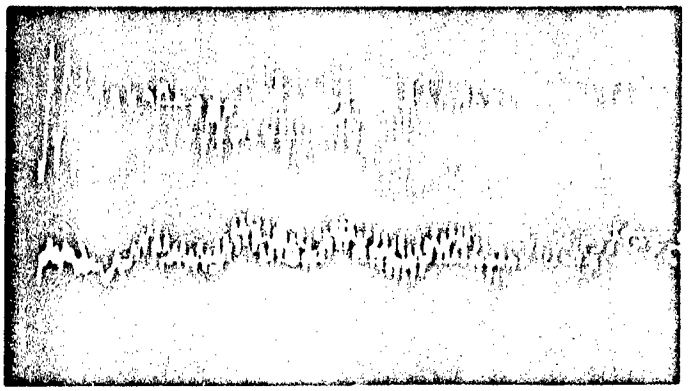

P_c = 50 psig, O/F = 10

Upper, P_c = 10 psi/div

Lower, P_i = 5 psi/div

Time = .5 ms/div

(b) 11 x .125 (333 fps) injection

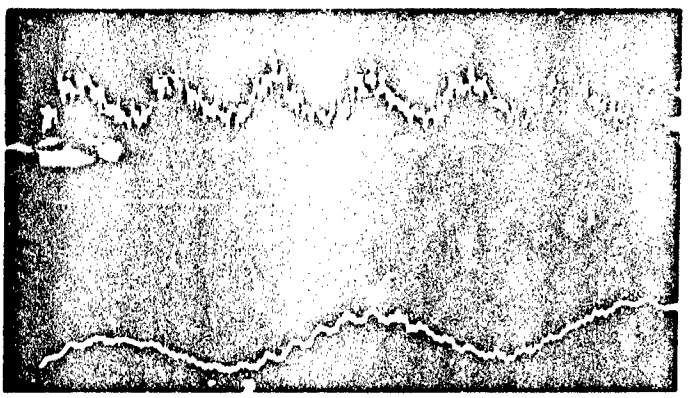

P_c = 100 psig, O/F = 10

Upper, P_c = 20 psi/div

Lower, P_i = 10 psi/div

Time = .5 ms/div

(c) 6 x .100 (922 fps) injection

Fig. 14. Simultaneous Records of Chamber Pressure (P_c) and Injector Upstream Pressure (P_i) for Different Injection Velocities. Uncooled Metal Chamber.

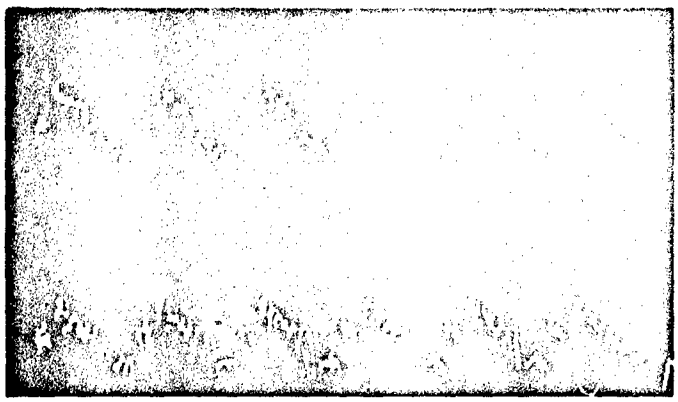

P_c = 100 psig, O/F = 10

Both traces,
P_c = 20 psi/div

Time = .5 ms/div

(a) 6 x .125 (594 fps) injection

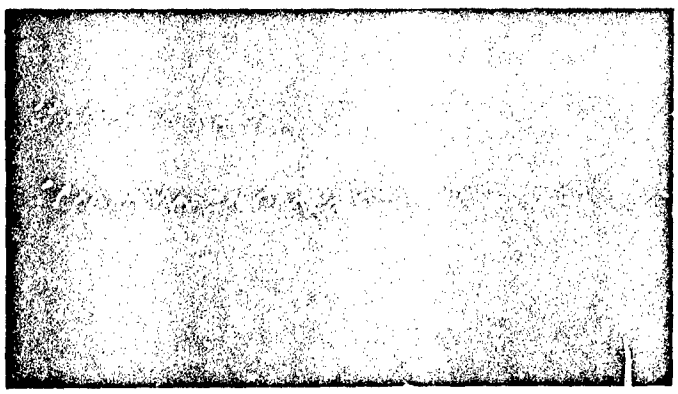

P_c = 50 psig, O/F = 10

Both traces,
P_c = psi/div

Time = .5 ms/div

(b) 12 x .125 (297 fps) injection

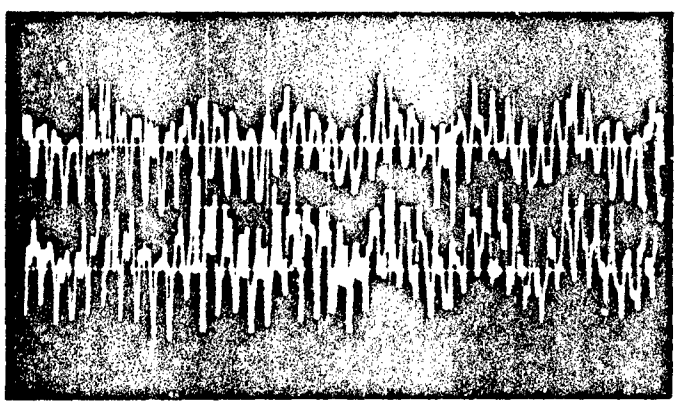

P_c = 100 psig, O/F = 10

Both traces,
P_c = 5 psi/div

Time = .5 ms/div

(c) 11 x .125 (333 fps) injection

Fig. 15. Simultaneous Chamber Pressure Records of Longitudinal and Transverse Oscillations in Uncooled Metal Chamber. Pickups 180° Apart on a Plane 2.8 inches from Injector.

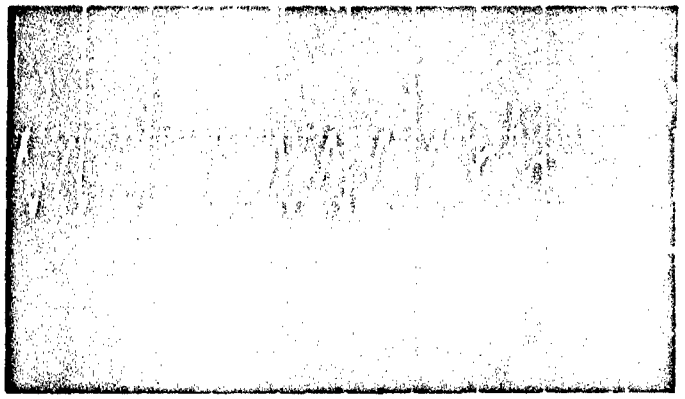

P_c = 100 psig, O/F = 9

P_c = 20 psi/div

Time = .2 ms/div

(a) 12 x .070 (943 fps) injection

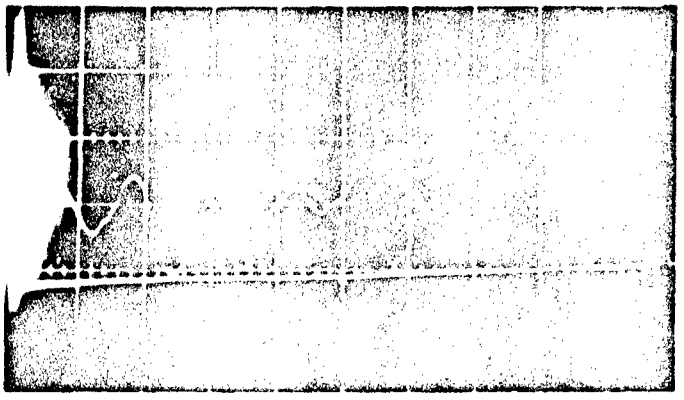

P_c = 125 psig, O/F = 7

Upper, P_c = 20 psi/div

Lower, OH = 500 mv/div

Time = .05 ms/div

(b) 4 x .125 (890 fps) A injection

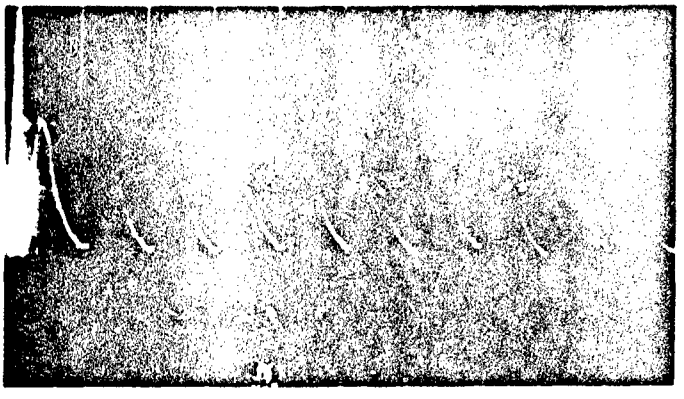

P_c = 125 psig, O/F = 7

P_c = 20 psi/div

Time = .1 ms/div

(c) 4 x .125 (890 fps) A injection

Fig. 16. Chamber Pressure Records (and one OH Emission Record) Showing Some Additional Transverse Oscillation Wave Forms in Uncooled Metal Chamber.

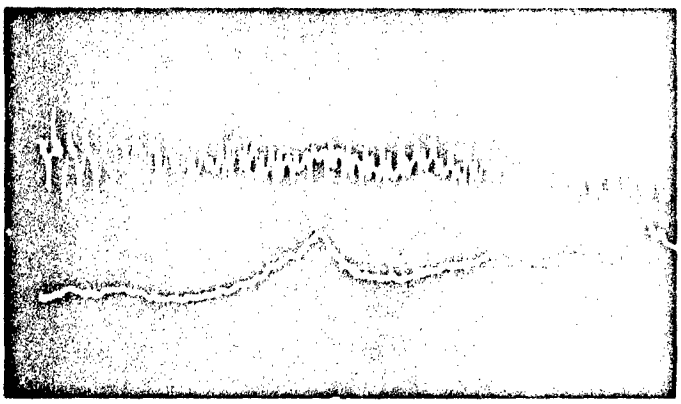

P_c = 100 psig, O/F = 10

Upper, P_c = 20 psi/div

Lower, Tot. Lum. = 50 mv/di

Time = .5 ms/div

(a) 11 x .125 (333 fps) injection

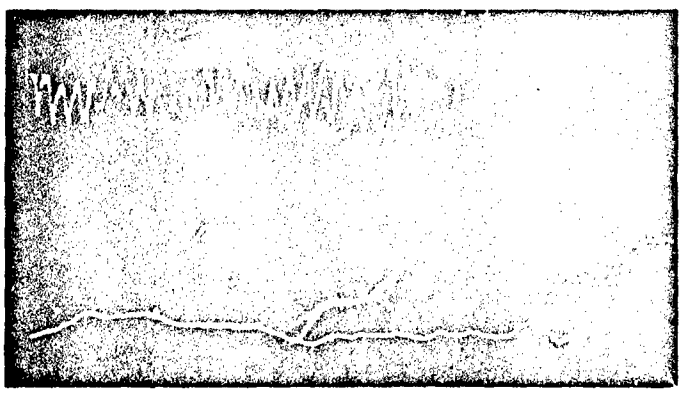

P_c = 75 psig, O/F = 9

Upper, P_c = 5 psi/div

Lower, CH = 200 mv/div

Time = .5 ms/div

(b) 11 x .125 (333 fps) injection

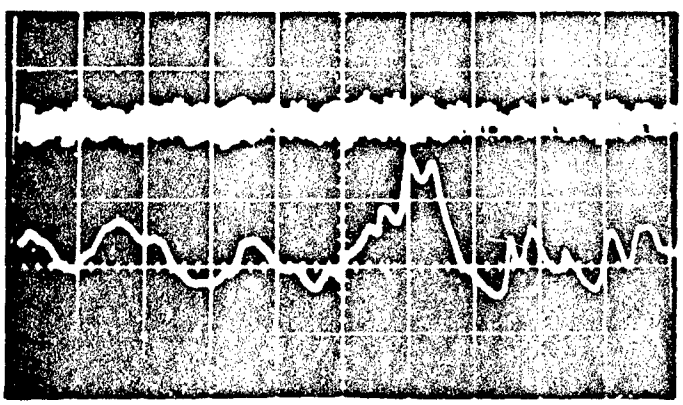

P_c = 125 psig, O/F = 8

Upper, P_c = 20 psi/div

Lower, OH = 100 mv/div

Time = 2 ms/div

(c) 4 x .125 (890 fps) A

Fig. 17. Simultaneous Records of Chamber Pressure and Light Emission (OH, CH and Total Luminosity): Transverse Oscillations. Uncooled Metal Chamber, (a) and (b); Water-Cooled Chamber, (c).

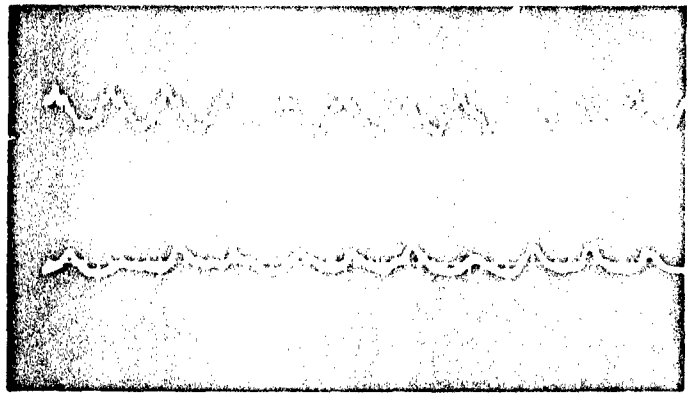

P_c = 50 psig, O/F = 10

Upper, P_c = 5 psi/div

Lower, OH = 20 mv/div

Time = 1 ms/div

(a) 11 x .125 (333 fps) injection

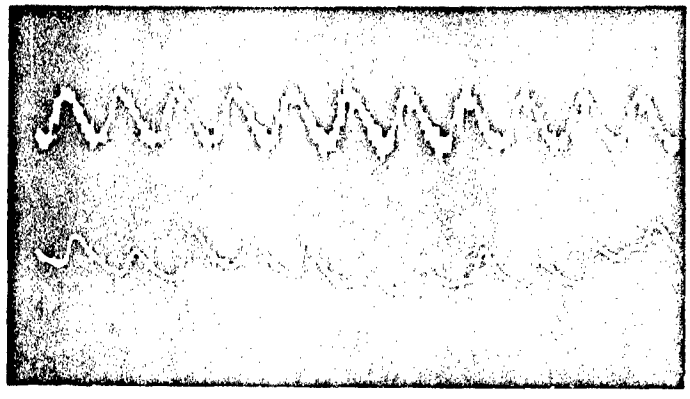

P_c = 50 psig, O/F = 10

Upper, P_c = 5 psi/div

Lower, CH = 100 mv/div

Time = 1 ms/div

(b) 11 x .125 (333 fps) injection

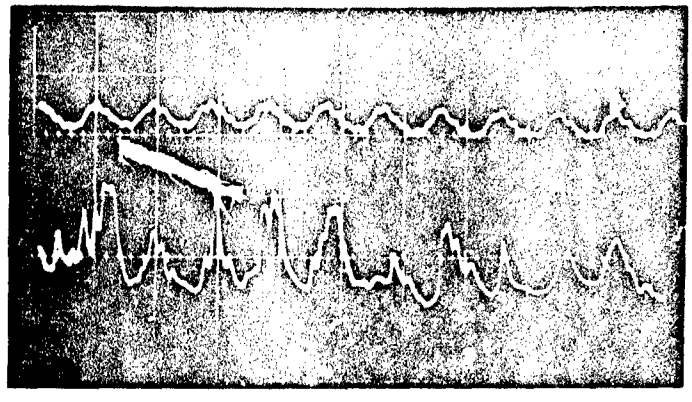

P_c = 50 psig, O/F = 10

Upper, P_c = 5 psi/div

Lower, Tot. Lum. = 100 mv/div

Time = 1 ms/div

(c) 11 x .125 (333 fps) injection

Fig. 18. Simultaneous Records of Chamber Pressure and Light Emission (OH, CH, and Total Luminosity): Longitudinal Oscillations with Subsonic Injection. Uncooled Metal Chamber.

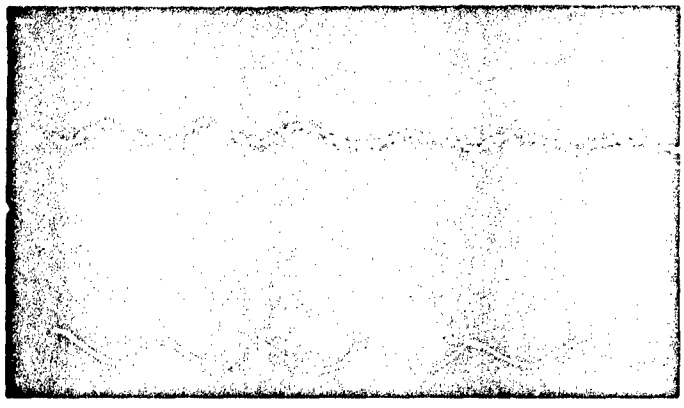

P_c = 100, O/F = 12

Upper, P_i = 20 psi/div

Lower, CH = 500 mv/div

Time = .5 ms

(a) 6 x .125 (594 fps) injection

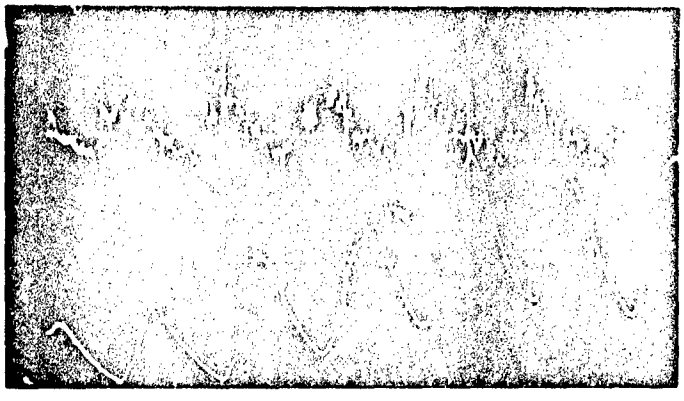

P_c = 100, O/F = 10

Upper, P_c = 20 psi/div

Lower, CH = 200 mv/div

Time = .5 ms

(b) 6 x .125 (594 fps) injection

P_c = 100, O/F = 12

Upper, P_c = 50 psi/div

Lower, CH = 500 mv/div

Time = .5 ms

(c) 6 x .125 (594 fps) injection

Fig. 19. Simultaneous Records of Upstream Injector Pressure, (a), or Chamber Pressure, (b) and (c), and CH Emission for Longitudinal Oscillations with Subsonic Injection. Uncooled Metal Chamber.

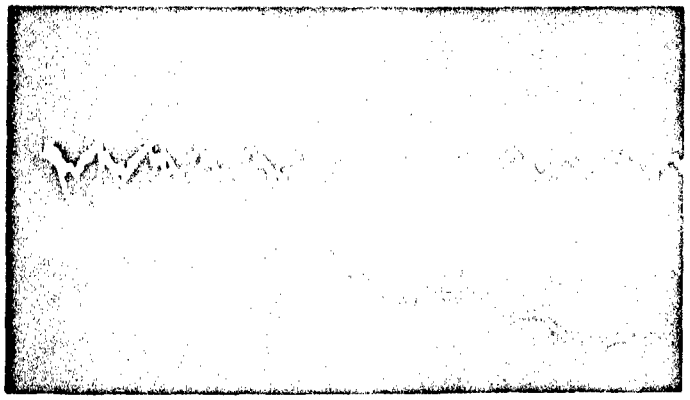

P_c = 50 psig, O/F = 10

Upper, P_c = 10 psi/div

Lower, OH = 50 mv/div

Time = 1 ms/div

(a) 6 x .100 (922 fps) injection

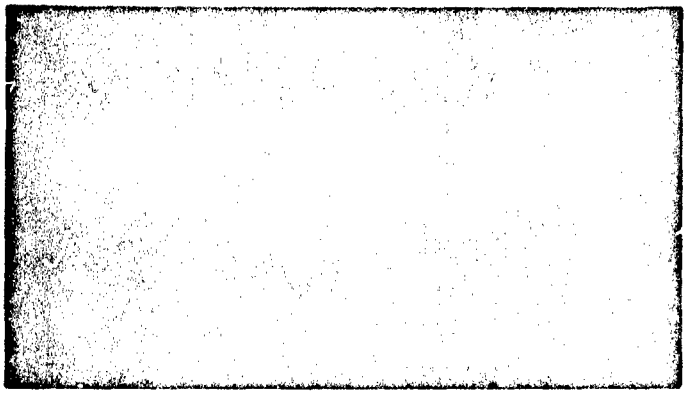

P_c = 50 psig, O/F = 10

Upper, P_c = 10 psi/div

Lower, CH = 500 mv/div

Time = 1 ms/div

(b) 6 x .100 (922 fps) injection

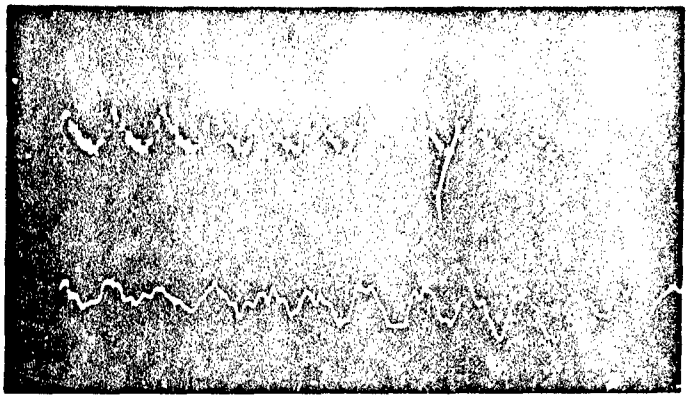

P_c = 50 psig, O/F = 10

Upper, P_c = 10 psi/div

Lower, Tot. Lum. = 100 mv/div

Time = 1 ms/div

(c) 6 x .100 (922 fps) injection

Fig. 20. Simultaneous Records of Chamber Pressure and Light Emission (OH, CH, and Total Luminosity) for Longitudinal Oscillations with Sonic Injection at 50 psig. Uncooled Metal Chamber.

P_c = 100, O/F = 10

Upper, P_c = 20 psi/div

Lower, OH = 500 mv/div

Time = 1 ms

(a) 6 x . 100 (922 fps) injection

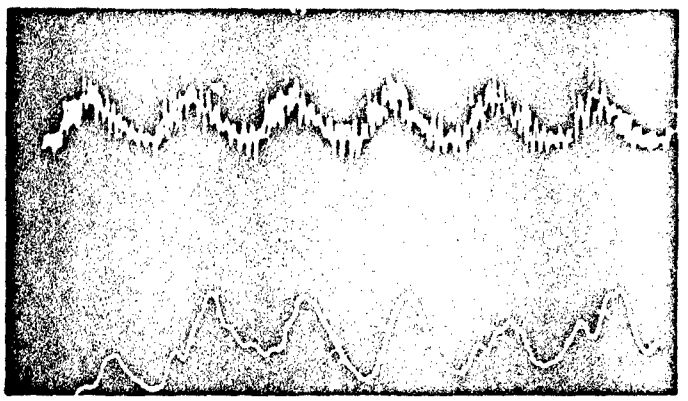

P_c = 100, O/F = 10

Upper, P_c = 20 psi/div

Lower, CH = 200 mv/div

Time = . 5 ms/div

(b) 6 x . 100 (922 fps) injection

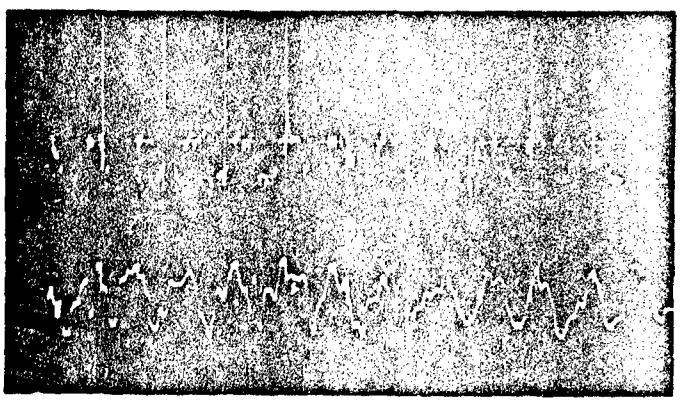

P_c = 100 psig, O/F = 10

Upper, P_c = 20 psi/div

Lower, Tot. Lum. = 100 mv/div

(c) 6 x . 100 (922 fps) injection

Fig. 21. Simultaneous Records of Chamber Pressure and Light Emission (OH, CH, and Total Luminosity) for Longitudinal Oscillations with Sonic Injection at 100 psig. Uncooled Metal Chamber.

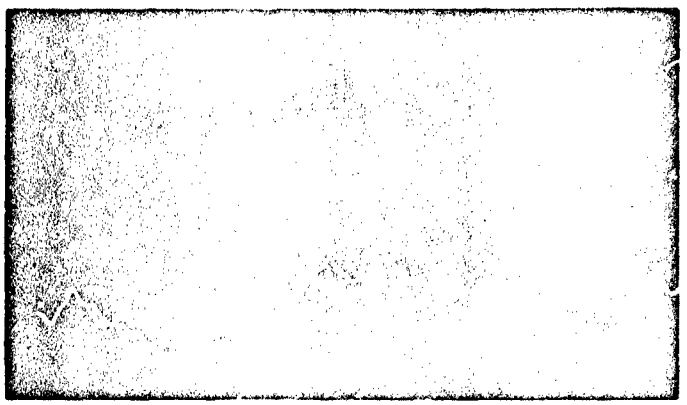

P_c = 150 psig, O/F = 10

Upper, P_c = 20 psi/div

Lower, OH = 500 mv/div

Time = 1 ms/div

(a) 6 x . 100 (922 fps) injection

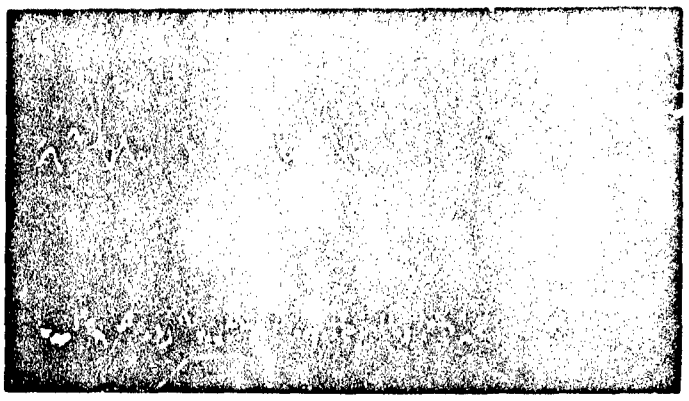

P_c = 150 psig, O/F = 10

Upper, CH = 200 mv/div

Lower, P_c = 50 psi/div

Time = 1 ms/div

(b) 6 x . 100 (922 fps) injection

Fig. 22. Simultaneous Records of Chamber Pressure and Light Emission (OH and CH) for Longitudinal Oscillations with Sonic Injection at 150 psig. Uncooled Metal Chamber.

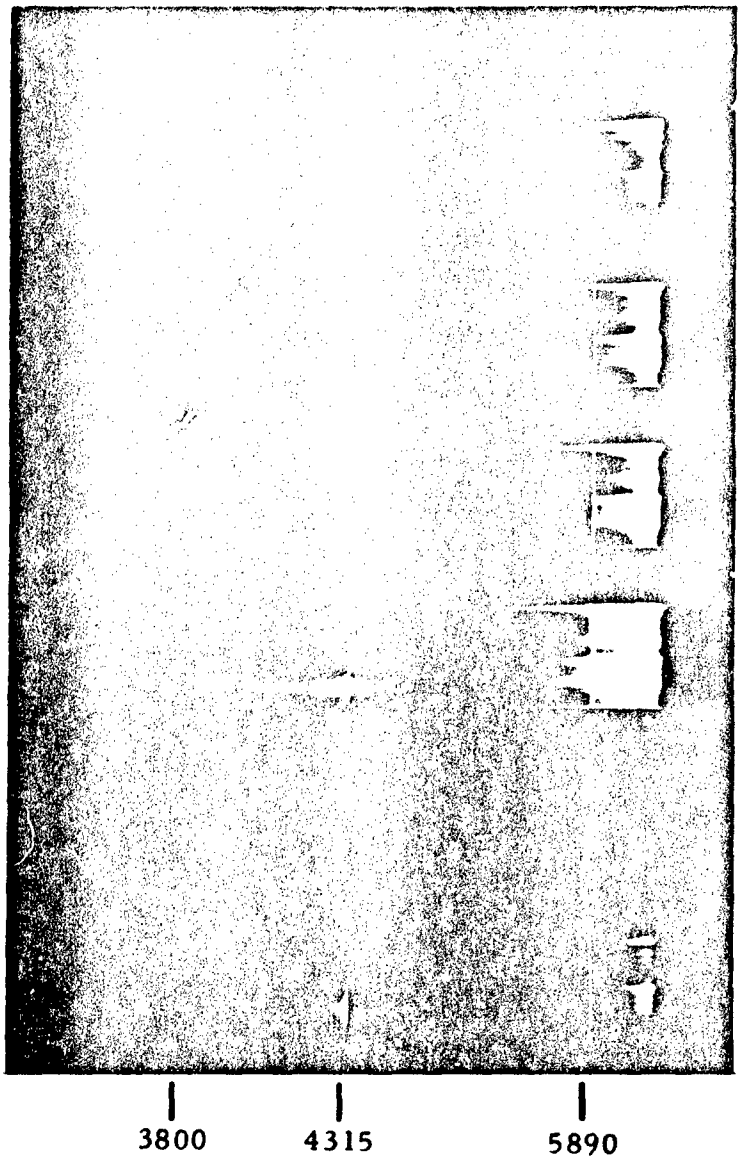

P_c (psig)	Slit Width
100	100 μ
100	200 μ
150	100 μ
150	200 μ
50	100 μ
50	200 μ

Fig. 23. Spectra of Visible Radiation from Combustion Chamber at Chamber Pressures (P_c) of 50, 100, and 150 psig.

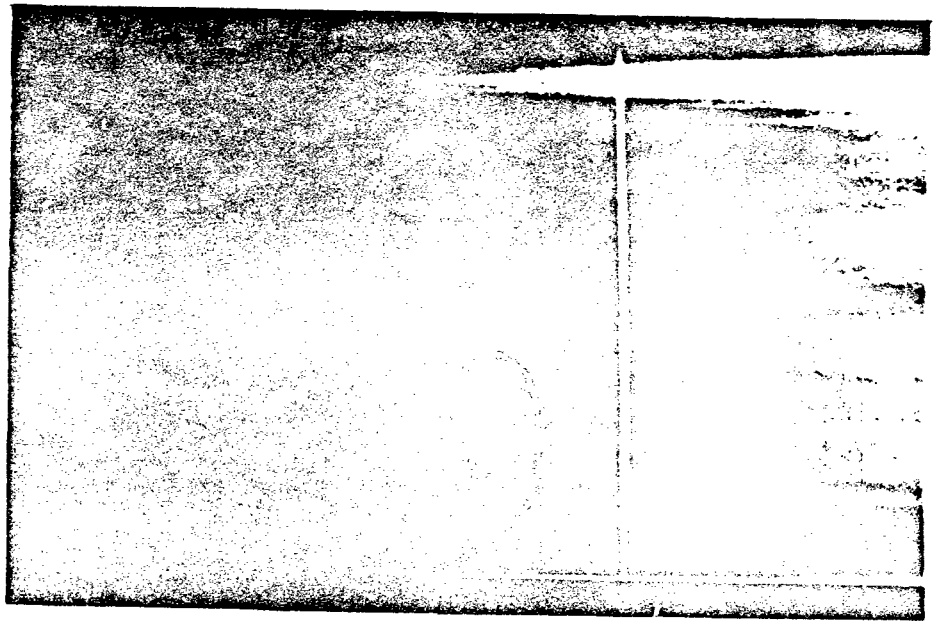

Striated Continuum of Spectrum (Figure 23)
at 150 psig, 100μ Slit.

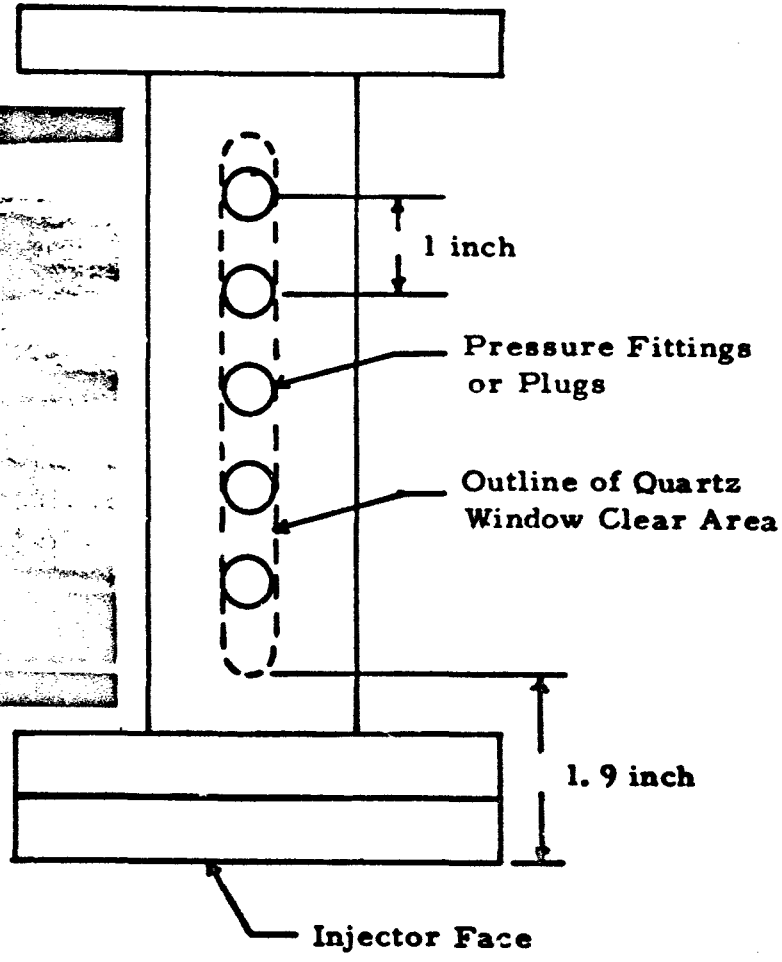

Fig. 24. Relationship of Striated Continuum to Chamber Window and to Arrangement of Pressure Tap Plate Opposite Window.

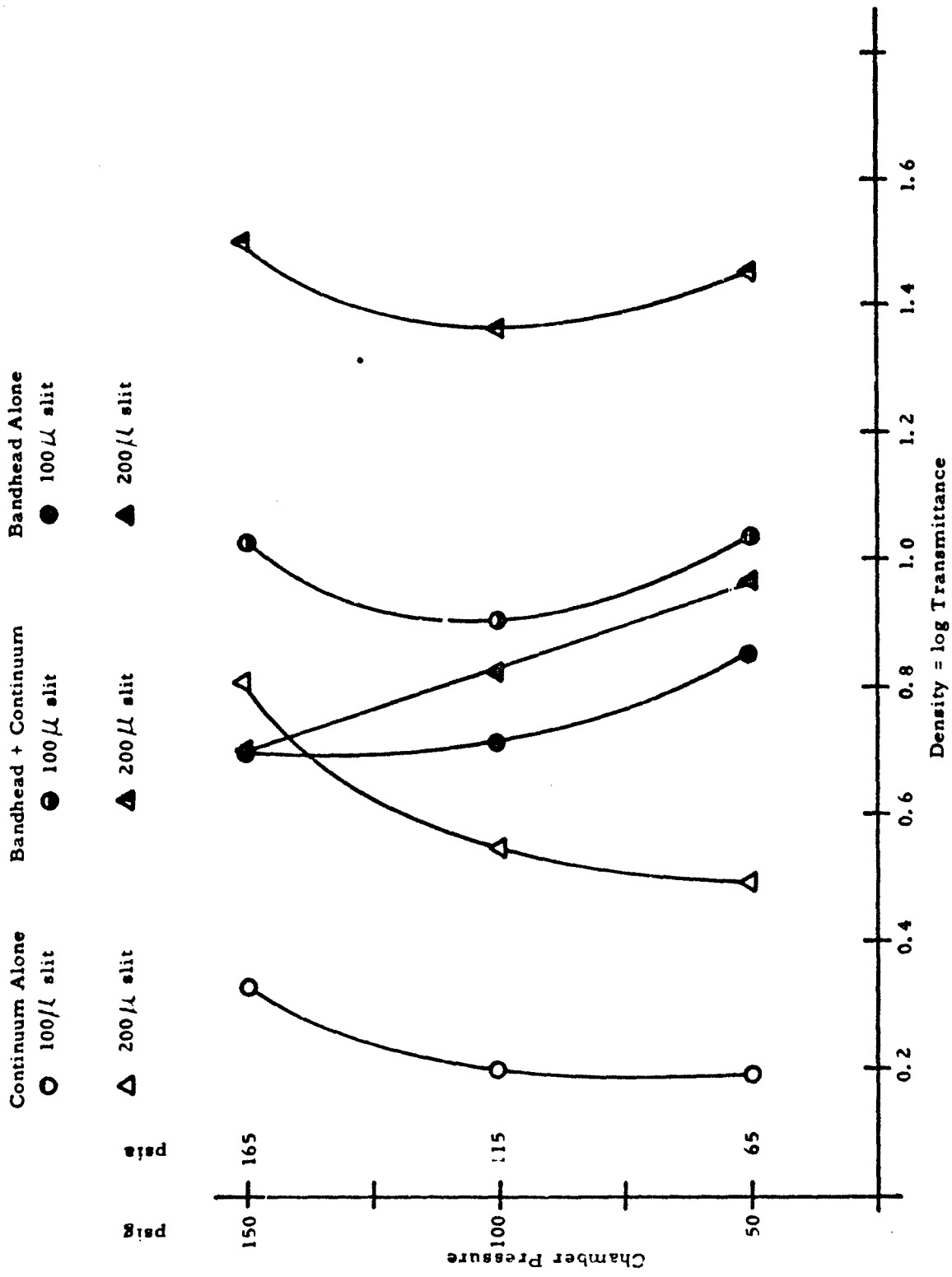

Fig. 25. Density vs Chamber Pressure of Visible Spectra (refer to Fig. 23) for CH Bandhead plus Continuum at 4315A. Continuum Alone and CH Bandhead Alone